Two-Dimensional Numerical Modeling and Design Optimization of a Moored Buoy Under Ice Load

Ruolin Cai

November, 2018

Master of Science Thesis

TU Delft Delft University of Technology

Two-Dimensional Numerical Modeling and Design Optimization of a Moored Buoy Under Ice Load

By

Ruolin Cai

Student number: 4521560

in partial fulfillment of the requirements for the degree of

Master of Science

in Offshore and Dredging Engineering

at the Delft University of Technology,

to be defended publicly on Thursday November 29, 2018 at 10:30 AM.

Thesis committee:	Prof. dr. A. Metrikine,	TU Delft
	Ir. J.S. Hoving,	TU Delft
	Dr. ir. K.N. van Dalen,	TU Delft
	Dr. M.A. van den Berg,	TU Delft

TU Delft Delft University of Technology

TU Delft Delft University of Technology

Cover picture retrieved from https://www.maritime-executive.com/.

PREFACE

With this thesis completed, I finished my incredible studying career in TU Delft, where I have been able to cultivate my interest and dedication to academic research. Furthermore, the international studying experience I gained broadens my horizons, which will further benefit me in my future career.

I would like to express my gratitude to my thesis committee members:

Prof.dr. A. Metrikine, the committee chairman and the head of Section Offshore Engineering, for having helped me finding an amazing thesis topic. His humorous way of teaching and his dedication to research have always impressed me in the past two years.

Ir. J.S. Hoving, the acting committee chairman, for his valuable comments and advise in all progress meetings I had, having encouraged me moving forward. He also helped me arrange every meeting and the graduation session, which I really appreciated.

Ir. M.A. van den Berg, my daily supervisor, who consistently steered me in the right direction. He gave me valuable feedback almost every week with great patience, even in his busy time in Norway, which helped me tremendously. Without his help, I wouldn't be able to finish my thesis.

Dr.ir. K.N. van Dalen, the external committee member, for having found time to be part of the thesis committee.

I wish to thank my parents for their continuous support and prayer since the beginning of this experience. Lastly, thanks to all my roommates, friends, and fellow students who made my life in the Netherlands more colorful.

Ruolin Cai
Delft, November 2018

SUMMARY

A single point mooring (SPM) system is one of the possible mooring systems in the field of Arctic floating production. It consists of a moored buoy to provide its anchoring unit with the capacity of mooring and ice sheltering. In the preliminary design phase, the performance of the mooring buoy must be assessed. This can be done by numerical modeling. This thesis provides a model for the two-dimensional numerical simulation of a moored buoy under ice loading, and it optimizes the buoy design based on the results of the numerical simulation.

The model is constructed based on the discrete element method (DEM), where the elements consist of the elements describing the level ice, and one element describing the buoy. The numerical model is capable of simulating several ice-structure interaction mechanisms, including the ice compressive failure, the ice bending failure, and friction.

The model consists of three parts. A compliant contact formulation describes the behavior of contacts between elements. Contact forces are solved implicitly using a Lagrange multiplier formulation. Lastly, the mooring system is described using the catenary equation.

The model is validated against a number of analytical solutions, demonstrating that the model is capable of simulating the buoy-ice interaction. An example of the buoy design optimization process is demonstrated. The optimization aims to obtain a concept design of a satisfactorily performing moored buoy with minimized dimensions under a specific ice condition. Design criteria were determined for the maximum pitch angle and the maximum horizontal displacement of the buoy. Given the desired design criteria, one can obtain the most optimized buoy design after several phases of selection.

CONTENTS

LIST OF FIGURES

LIST OF TABLES

List of Symbols

$\mathbf{A}$	Dominant matrix
$\mathbf{A}_0$	Dominant matrix derived without compliance factors
A_c	Contact area
A_i	(Side) sectional area of the level ice
A_m	Cross sectional area of a mooring line
A_s	(Side) sectional area of the buoy
$\mathbf{a}_{ex}$	Explicit acceleration vector
$\mathbf{B}$	Multiplier vector
$\mathbf{B}_i$	Multiplier vector of the level ice
b_i	Width of the level ice
$\mathbf{C}$	Vector of damping coefficients
$c_{d,f,i}$	Form drag coefficient of the level ice
$c_{d,s,i}$	Skin friction coefficient of the level ice
$c_{d,f,s}$	Form drag coefficient of the buoy
$c_{d,s,s}$	Skin friction coefficient of the buoy
CF	Compliance factor
CF_c	Compliance factor of the contact
$\mathbf{CF}$	Vector of compliance factors
$D_{m,a}$	Distance between the anchor and the initial touchdown point
$D_{s,max}$	Maximum diameter of the buoy
$D_{s,min}$	Minimum diameter of the buoy
$D_{s,wl}$	Waterline diameter of the buoy
d_i	Draft of the level ice
d_m	Distance between the fairlead and the seabed
$d_{m,f}$	Distance between the fairlead and the bottom edge of the buoy
d_r	Relative distance between two contact points
d_s	Draft of the buoy
d_w	Water depth
$\mathbf{E}$	Contact matrix
$\mathbf{E}_c$	Contact matrix (vector) of the ice-structure contact
$\mathbf{E}_i$	Contact matrix (vector) of the level ice
E_i	Young's modulus of the level ice
$\mathbf{F}_{im}$	Vector of (average) implicit forces
$\mathbf{F}_{ex}$	Vector of explicit forces
F_c	Contact force
$F_{D,f,i}$	Form drag force of the level ice
$F_{D,f,s}$	Form drag force of the buoy
$F_{D,i}$	Total drag force of the level ice
$F_{D,s}$	Total drag force of the buoy
$F_{D,s,i}$	Skin Friction drag force of the level ice
$F_{D,s,s}$	Skin Friction drag force of the buoy
F_f	Friction
F_m	Tension of a mooring line
$F_{m,x}$	Normalized horizontal tension component of a mooring line
$F_{m,y}$	Downward pull force induced by mooring lines
$F_{R,L}$	Linear component of the mooring restoring force
$F_{R,NL}$	Non-linear component of the mooring restoring force

F_R	Mooring restoring force
F_{x1}	Horizontal component of the tension on the #1 fairlead
F_{x2}	Horizontal component of the tension on the #2 fairlead
F_{y1}	Vertical component of the tension on the #1 fairlead
F_{y2}	Vertical component of the tension on the #2 fairlead
f_b	Flexural stress
G_i	Shear modulus of the level ice
g	Gravity acceleration
H_s	Height of the buoy
$I_{n,i}$	Moment of area of the level ice element
$I_{n,s}$	Moment of area of the buoy
$I_{t,i}$	Second moment of area of the level ice
$I_{t,s}$	Second moment of area of the buoy
l_i	Length of the level ice element
$\mathbf{K}$	Vector of stiffnesses
$k_{b,i}$	Equivalent buoyancy stiffness of the level ice
$k_{b,s}$	Equivalent buoyancy stiffness of the buoy
k_c	Ice-structure contact stiffness
$k_{n,i}$	Ice-ice normal (horizontal) contact stiffness
$k_{r,i}$	Ice-ice rotational contact stiffness
$k_{t,i}$	Ice-ice sheer (vertical) contact stiffness
k_R	Equivalent restoring stiffness
L_m	Total length of the mooring chain
$\mathbf{M}$	Inertia matrix
$\mathbf{M}_i$	Inertia matrix of the level ice
M_b	Bending moment
M_H	Heeling moment
M_m	Righting moment induced by mooring lines
M_R	Total restoring moment
M_S	Righting moment induced by the hydrostatic stability
N	Element number
N_i	Ice element number
$n_{c,i}$	Total number of contact constraints of the level ice
$n_{dof,i}$	Total number of degrees of freedom of the level ice
$\mathbf{m}$	Inertia vector
m_s	Weight of the buoy
$\mathbf{RHS}$	Right-hand-side vector
$\mathbf{RHS}_i$	Right-hand-side vector of the level ice
$R_{g,s}$	Radius of gyration of the buoy
Re_i	Reynolds number of the level ice
S_i	Salinity of the sea ice
S_m	Length of a suspended mooring line
S_s	Surface area of the buoy
$\mathbf{T}$	Compliance matrix
$\mathbf{T}_i$	Compliance matrix of the level ice
T	Shear force
T_i	Average ice temperature
t_i	Thickness of the level ice
t_s	Equivalent hull thickness of the buoy
$\mathbf{u}$	Displacement vector

$\dot{\mathbf{u}}$	Velocity vector
u	Displacement
$\dot{u}$	Velocity
$\dot{u}_{\mathrm{i}}$	Velocity of the level ice
$\dot{u}_{\mathrm{r}}$	Relative velocity of two contact points
$\dot{u}_{\mathrm{r,av}}$	Average relative velocity of two contact points
$\dot{u}_{\mathrm{s}}$	Velocity of the buoy
$V_{\mathrm{d,s}}$	Displaced water volume of the buoy
$v_{\mathrm{b,i}}$	Brine volume fraction of the sea ice
w_{m}	Unit weight of a mooring line
X_{m}	Horizontal distance between the fairlead and the touchdown point
x_{bl}	Breaking length of the level ice
α	Downward-sloping hull angle of the buoy
β	Contact angle
Δt	Length of time-step
$\boldsymbol{\Delta\dot{\mathbf{u}}}$	Velocity variation vector
$\boldsymbol{\Delta\dot{\mathbf{u}}}_{\mathrm{ex}}$	Explicit velocity variation vector
$\boldsymbol{\Delta\dot{\mathbf{u}}}_{\mathrm{im}}$	Implicit velocity variation vector
δ	Overlapping distance (Penetration)
δ_{max}	Maximum penetration
θ	Upward-sloping hull angle of the buoy
$\boldsymbol{\lambda}$	Impulse vector
λ_{c}	Contact impulse
$\lambda_{\mathrm{c,max}}$	Maximum contact impulse
μ	Friction coefficient
μ_{w}	Dynamic viscosity of the sea water
ν	Poisson's ratio of the sea ice
ρ_{i}	Density of the sea ice
ρ_{m}	Submerged density of the mooring line material
ρ_{s}	(Average) density of the buoy material (steel)
ρ_{w}	Density of the sea water
$\sigma_{\mathrm{c,i}}$	Compressive strength of the sea ice
$\sigma_{\mathrm{f,i}}$	Flexural strength of the sea ice
φ	Pitch angle

1

INTRODUCTION

1.1 Background

When designing an offshore floating structure for Arctic regions, the potential presence of sea ice and the harsh climate are challenging engineering problems. Under such circumstances, a suitable mooring system is beneficial for stabilizing and reinforcing the floating structure while developing an Arctic oil field. Generally, there are several different kinds of mooring system in the field of offshore engineering, including but not limited to: the catenary mooring system, the taut leg mooring system, the tension leg (TL) mooring system, and the single point mooring (SPM) systems. An SPM system refers to a fixed or floating structure anchored offshore, which serves as a mooring and interconnect point. Figure 1-1 shows a tanker moored to an SPM system.

Figure 1-1 Tanker moored to an SPM system (SOFEC, 2009)[1]

In the scope of Arctic floating production, one of the most efficient mooring strategies is to employ a single buoy mooring system, which is one of the types of single point mooring systems. Overall, the single buoy mooring system consists of a permanently moored buoy, to which the offshore unit is connected. The moored buoy itself is usually moored with the catenary mooring system, which is currently one of the most commonly applied mooring systems.

One of the advantages regarding applying the buoy system is that the moored floating structure is able to weathervane in 360° around the buoy and find a stable position with the minimum environmental loads. Additionally, in Arctic regions, the buoy is capable to block a part of the ice floes, which further reduces the impact of ice floes on the floating structure.

To survive the harsh Arctic environment, the buoy system is necessary to meet the requirement of strength and stability. This includes the design of the buoy itself, as well as the flexible configuration of its mooring system.

The most critical issue during Arctic oil production is usually the interaction between the structures and the sea ice. Under an overwhelming ice load, a floating structure may have a significant displacement and suffer damages on its structure, which is harmful for its operation. For smaller structures like a buoy, substantial ice loads may also cause a large angle of inclination, or may even submerge the buoy, causing damages to its mechanical components on deck. To avoid such accidents, also due to the low accessibility in the Arctic environment, a precise load prediction during the stage of design is imperative. The prediction of ice load and the interaction should be accurate and timely enough so that the possibility of the accidents and the frequencies of the maintenance and possible replacement during operation can be reduced.

Compared with the wind, wave, and current load prediction, the ice load prediction has much higher uncertainty. There are four different methods which are currently used by the arctic industry for the ice load predictions: design codes, full-scale measurement, model testing, and numerical simulation.

In the design process, ice-structure interactions to be considered may consist of managed ice, level ice, rubble fields, and ridged ice. Assessment of ice actions has always been a challenging topic. However, it is possible to simulate the interactions between the ice and structure numerically using discrete modeling consisting of both the ice and structure.

During the stage of concept design, two-dimensional modeling together with the dynamic simulation is an effective method to predict the ice-structure interaction. Since in the SPM system, a considerable percentage of ice load acts on the buoy, this thesis will focus on the numerical simulation of two-dimensional models of the moored buoy, under a specific ice load. Note that the interaction between the buoy system and its anchoring floating structure is not discussed in the thesis. An overview of one possible model is depicted in Figure 1-2.

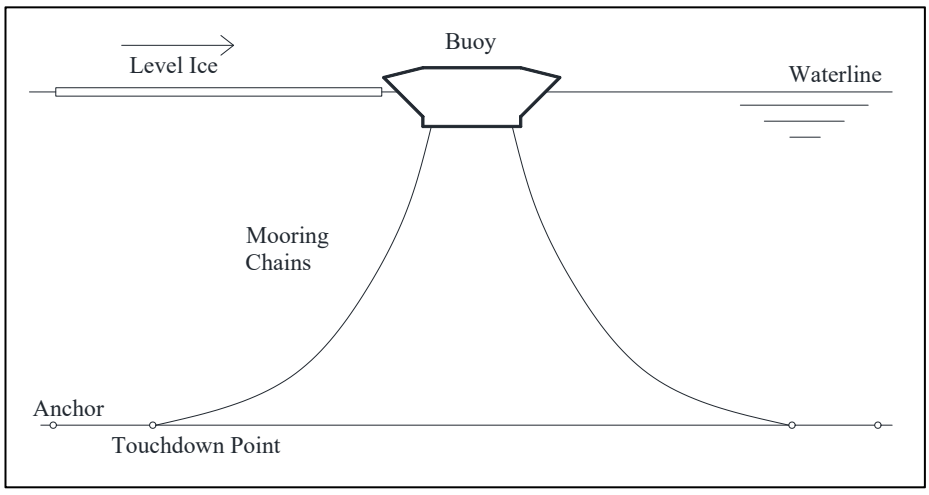

Figure 1-2 A concept model of the level ice and moored buoy

The concept model shows that, in a two-dimensional view, the buoy is anchored by two mooring chains; on the left side of the buoy, level ice is moving towards the buoy, and on the right side of the buoy, there is free water surface and no presence of ice.

To focus only on the influence of ice load on the buoy, the model will be assumed located at a leeward of the Svalbard Archipelago, Norway, where only the first-year ice is considered. The wind load and other environmental load are considered the minor influence on the model, which can be ignored during the simulation. The location of the Svalbard Archipelago is indicated in dark green in Figure 1-3[2].

Figure 1-3 The location of the Svalbard Archipelago

The current study uses MATLAB as the primary tool of the simulation, which is capable to obtain relatively accurate predictions.

1.2 Thesis Objective

The primary objective of the present study is:
'To investigate the interaction between the level ice and the moored buoy, and optimize the buoy dimensions based on the numerical simulation'

Discrete modeling and time-domain analysis performed by MATLAB are used to analyze the interaction between the level ice and the moored structure.

To achieve the primary objective, the following sub-objectives are considered:
1. To determine the theories and methods employed in the numerical model;

2. To construct the numerical model that consists of the level ice model, the moored buoy model, and the interaction between the above two models;
3. To perform a series of determination of model parameters;
4. To verify the numerical model based on the simulation results;
5. To optimize the buoy with further simulations.

1.3 Thesis Outline

This thesis is structured into seven chapters. The outline of the thesis is given below:

Chapter 2 provides the theoretical basis on the method for model construction in the current study.

Chapter 3 describes the construction of the numerical model, which includes the detailed derivation of the model.

Chapter 4 carries out the determination of model parameters, where the preliminary input parameters of the model will be determined.

Chapter 5 performs a series of verification according to the results from the numerical simulation.

Chapter 6 presents the results obtained from the model, as well as the optimization of the designed structure based on the result.

Chapter 7 draws the conclusions of the thesis together with the recommendation for future research.

2

THEORY OF MODEL CONSTRUCTION

This chapter provides a brief overview of methods for constructing the model of level ice, the moored structure (refers specifically to the moored buoy in this thesis), as well as the contact mechanism between the level ice and moored structure. The first part of this chapter focuses on the compliant contact algorithm, a variant of the non-smooth discrete element method (NDEM), which is the main theory of the numerical model. The second part of this chapter introduces the Lagrange multiplier formulation, the primary method of the model derivation and numerical calculation. And finally, the third part of this chapter discusses the modeling theory of mooring lines.

2.1 Introduction

Since the purpose of the numerical model is to simulate the behavior for both the level ice and moored structure, the result should be able to reflect the real-life situation as accurately as possible. Therefore, the choices of model construction methods are supposed to suit the specific physical characteristics and the status of the contact. In particular, during the contact between the level ice and buoy, the level ice usually fails both due to crushing and bending, while the buoy usually deviates from its original position and tilts with a significant angle.

Based on the situation described above, the level ice should be modeled as a non-rigid body since we focus on its deformation, while the moored structure can be modeled as a rigid body since we investigate its motions. Moreover, the ice-structure interaction should be observed micro-mechanically, which is also considered as a non-continuous problem. Under this circumstance, the discrete element method (DEM) is presented for modeling the current system, since compared with the finite element method (FEM), it focuses more on the micro-mechanical interactions of the elements, and it allows the model to further include the mechanic of broken ice. Furthermore, there are two different branches for this method, namely the smooth discrete element method (SDEM) and non-smooth discrete element method (NDEM). The SDEM is computationally more efficient for soft materials, wide and tall systems, and with increasing flow rate, while the NDEM is more beneficial for stiff materials, shallow systems, static or slow flow[3]. In the current system, both the level ice and structure can be considered as stiff materials, and the flow can be considered static or slow. Therefore, the NDEM is considered more suitable than SDEM in the current study.

The contacts between elements in the current system are compliant, which indicates the elements are not rigidly connected to each other. For instance, the level ice may break due to failure, and even when it is not broken, there is still displacement between adjacent elements because of the elastic deformation of the ice sheet. The

moored structure model is not connected to any ice element, and they will only interact when contacting with each other. Therefore, in general, any contact in the system is considered as the compliant contact. To process the compliant contact, it is necessary to apply the compliant contact algorithm, which is a variant of the NDEM. We will further discuss this algorithm in detail in Section 2.2.

To apply the above algorithm into the model and to generally make sure that the numerical simulation is well performed and optimized, an appropriate solution is the Lagrange multiplier formulation. The Lagrange multiplier formulation is a method for finding the local maxima and minima of a function subject to equality constraints. The detailed derivation will be introduced in Section 2.3.

Another essential component of the system is the mooring line, which is connected to the buoy structure. The current study analytically models mooring lines, which is based on the catenary mooring system. The description of the related theory is illustrated in Section 2.4.

2.2 Compliant Contact Algorithm

2.2.1 Contact Overview

When dealing with the compliant contacts between elements, especially the contact between the ice and structure, there are several problems we will encounter. One of the problems is the positioning of the contact points (one on each element), considering that the contact points are not constant due to the elements rolling and sliding over each other. Generally, the contact points are considered to have the smallest distance between them. A typical schematic is depicted in Figure 2-1.

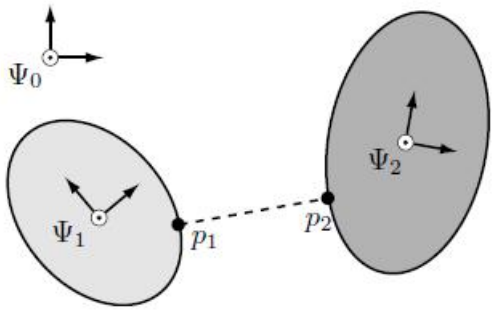

Figure 2-1 Two rigid bodies and their generalized contact points p_1 and p_2[4]

Noted that in the current study, the positioning of contact points is only necessary when dealing with ice-structure contact, while the contact points between adjacent ice elements are considered fixed, which means when dealing with the ice-ice contact, two adjacent elements can be regarded as merely connected at specific connect points, therefore its positioning process can be neglected. The detailed positioning process will be discussed in Chapter 3.

Another critical difficulty is associated with the evaluation of contact parameters, namely the contact stiffness and damping coefficient. Generally, in a two-dimensional plane, any adjacent ice elements are assumed connected with constraints in three degrees of freedom (horizontal, vertical, and rotational). These constraints are defined

by contact stiffnesses and damping coefficients, which can be evaluated analytically or experimentally. The process of evaluation will be explained in Chapter 4.

2.2.2 Compliance Factor

To describe the extent of compliance between two elements, the compliance factor is introduced. This is considered the core coefficient of the compliant contact algorithm, which is applied throughout the process of the numerical model, by substituting into the Lagrange multiplier formulation.

The compliance factor is derived as below:

The derivation starts from a simplest model: a shapeless mass connected to the fixed boundary with a spring and a damper. A sketch is depicted in Figure 2-2.

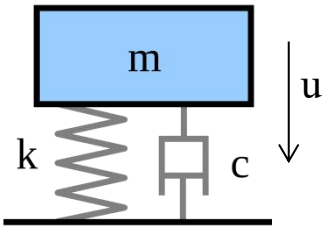

Figure 2-2 A shapeless mass connected to fixed boundary with a spring and a damper

Force in contact at the beginning of a time step:

$$F_{\mathrm{n}} = -ku - c\dot{u} \tag{2-1}$$

Force in contact at the end of a time step:

$$F_{\mathrm{n+1}} = -k\left(u + \dot{u}\Delta t + \frac{1}{2}\Delta\dot{u}\Delta t\right) - c\left(\dot{u} + \Delta\dot{u}\right) \tag{2-2}$$

Using Newmark-Beta method[5] with γ = 0.5 and β = 0.25, yielding the constant average acceleration method (2nd order). Average force over a time step:

$$F_{\mathrm{av}} = (1-\gamma)F_{\mathrm{n}} + \gamma F_{\mathrm{n+1}} \tag{2-3}$$

Substitution gives:

$$F_{\mathrm{av}} = -\frac{ku + c\dot{u} + k\left(u + \dot{u}\Delta t + \frac{1}{2}\Delta\dot{u}\Delta t\right) + c\left(\dot{u} + \Delta\dot{u}\right)}{2} \tag{2-4}$$

The impulse applied during a time step is:

$$\lambda = F_{\mathrm{av}} \cdot \Delta t \tag{2-5}$$

Combining this with (2-4), and rewriting gives:

$$-\lambda = k\left(u\Delta t + \frac{1}{2}\dot{u}\Delta t^2 + \frac{1}{4}\Delta\dot{u}\Delta t^2\right) + c\left(\dot{u}\Delta t + \frac{1}{2}\Delta\dot{u}\Delta t\right) \tag{2-6}$$

Since:

$$\lambda = m\Delta\dot{u} \tag{2-7}$$

substituting (2-7) into (2-6), we obtain:

$$-\left(m+\frac{1}{4}k\Delta t^2+\frac{1}{2}c\Delta t\right)\Delta\dot{u} = k\left(u\Delta t+\frac{1}{2}\dot{u}\Delta t^2\right)+c\dot{u}\Delta t \tag{2-8}$$

The equation now solves for the velocity variation of the body. Alternatively, one could also solve for the contact impulse within the time step. Substituting (2-7) into (2-8) gives:

$$-\left(m+\frac{1}{4}k\Delta t^2+\frac{1}{2}c\Delta t\right)\frac{\lambda}{m} = k\left(u\Delta t+\frac{1}{2}\dot{u}\Delta t^2\right)+c\dot{u}\Delta t \tag{2-9}$$

which can be rewritten as:

$$-\left(1+\frac{1}{m}\left(\frac{1}{4}k\Delta t^2+\frac{1}{2}c\Delta t\right)\right)\lambda = (k\Delta t)u+\left(\frac{1}{2}k\Delta t^2+c\Delta t\right)\dot{u} \tag{2-10}$$

or the formulation as below:

$$-\left(\frac{1}{m}+\frac{1}{\frac{1}{4}k\Delta t^2+\frac{1}{2}c\Delta t}\right)\lambda = \frac{k}{\frac{1}{4}k\Delta t+\frac{1}{2}c}u+2\dot{u} \tag{2-11}$$

The equation above is the core equation for the compliant contact algorithm, from here the compliance factor can be determined by specific stiffness and damping coefficients, as well as the length of time step:

$$CF = \frac{1}{\frac{1}{4}k\Delta t^2+\frac{1}{2}c\Delta t} \tag{2-12}$$

Thus, the core equation can be also written as:

$$\lambda\cdot CF+\Delta\dot{u} = -k\cdot u\cdot CF\cdot\Delta t-2\dot{u} \tag{2-13}$$

2.3 Lagrange Multiplier Formulation

Since the compliance factor is obtained, we can apply it to solve a model with complex contact situations, and the approach implemented here is the Lagrange multiplier formulation. The advantage of this approach is that it allows the optimization to be solved without explicit parameterization regarding the constraints. In this formulation, Lagrange multipliers are computed by solving a matrix equation:

$$\mathbf{E}\mathbf{M}^{-1}\mathbf{E}^{\mathrm{T}}\mathbf{B} = \mathbf{c} \tag{2-14}$$

where the vector **B** contains the multipliers that we wish to solve for, and **M** is a block-diagonal matrix. The vector **c** expresses the forces applied to the elements. **E** is the Jacobian matrix, which includes the information on the constraints' connectivity[6]. While the size of block-diagonal matrices depends on the degrees of freedom in the system.

To specify the formulation into our model, it can be rewritten as below:

$$\begin{bmatrix} \mathbf{M} & -\mathbf{E} \\ \mathbf{E}^{\mathrm{T}} & \mathbf{T} \end{bmatrix} \begin{bmatrix} \Delta\dot{\mathbf{u}}_{\mathrm{im}} \\ \boldsymbol{\lambda} \end{bmatrix} = \begin{bmatrix} \mathbf{0} \\ \mathbf{RHS} \end{bmatrix} \tag{2-15}$$

The formulation can also be written as:

$$\begin{aligned} &\left(\mathbf{E}^{\mathrm{T}}\mathbf{M}^{-1}\mathbf{E}+\mathbf{T}\right)\cdot\boldsymbol{\lambda}=\mathbf{RHS} \\ &\Delta\dot{\mathbf{u}}_{\mathrm{im}}=\mathbf{E}\boldsymbol{\lambda}\circ\mathbf{m}^{\circ-1} \end{aligned} \tag{2-16}$$

where the symbol "$\circ$" represents the Hadamard product (also known as the entrywise product)[7].

In the following sections, the detailed explanations of each term in the formulation will be presented.

2.3.1 Contact Matrix **E**

The contact matrix (noted as **E**) contains the contact information regarding all degrees of freedom. To simplify the explanation, we assume a system with three elements in a two-dimensional plane, where the length of each element is *L*. The three elements contact with their adjacent elements in fixed contact points (at the center of ends along the length), which according to compliant contact theory, are assumed connected with equivalent springs and dashpot in all three degrees of freedom (horizontal, vertical, and rotational). A concept map of the connections between adjacent elements is depicted in Figure 2-3.

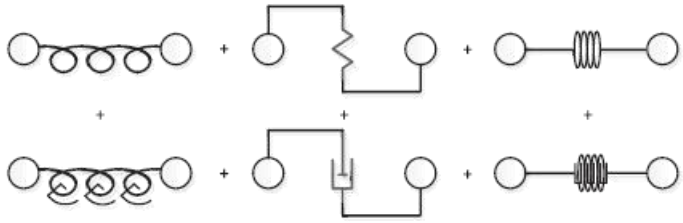

Figure 2-3 Concept map of the connection between adjacent elements

The left end of the first element (M_1) and the right end of the third element (M_3) are free ends, see Figure 2-4.

Figure 2-4 A simple contact system with three elements

As we can observe from Figure 2-3 and 2-4, there are in total six contact constraints in the system. For each degree of freedom of each element, an equation can be derived regarding the influence of impulses at the contact points:

$$\begin{aligned} &m_1\Delta\dot{x}_1=-\lambda_{1,x} && m_1\Delta\dot{y}_1=-\lambda_{1,y} && I_{\mathrm{n},1}\Delta\dot{r}_1=-\frac{L}{2}\lambda_{1,y}-\lambda_{1,r} \\ &m_2\Delta\dot{x}_2=\lambda_{1,x}-\lambda_{2,x} && m_2\Delta\dot{y}_2=\lambda_{1,y}-\lambda_{2,y} && I_{\mathrm{n},2}\Delta\dot{r}_2=-\frac{L}{2}\lambda_{1,y}+\lambda_{1,r}-\frac{L}{2}\lambda_{2,y}-\lambda_{2,r} \\ &m_3\Delta\dot{x}_3=\lambda_{2,x} && m_3\Delta\dot{y}_3=-\lambda_{2,y} && I_{\mathrm{n},3}\Delta\dot{r}_3=-\frac{L}{2}\lambda_{2,y}+\lambda_{2,r} \end{aligned} \tag{2-17}$$

where m is the mass of the element, I_n the inertia of the element, $\Delta\dot{x}$ the velocity variation in the horizontal direction, $\Delta\dot{y}$ the velocity variation in the vertical direction, $\Delta\dot{r}$ the velocity variation in the rotational direction, L the length of an element, and λ is the impulse induced on the contact constraint, while the subscripts indicate the numbering of the elements.

Generally, on the left-hand side of the equations, for each element, there is its mass (inertia) multiplied by the velocity change (in a time-step) at a specific degree of freedom; while on the right-hand side, all relating impulses on its contact points are summed.

Now we can summarize the contact situation of the system as the table below. Each row corresponds to each degree of freedom of each element, while each column corresponds to each contact constraint.

	$I_{1,x}$	$I_{1,y}$	$I_{1,r}$	$I_{2,x}$	$I_{2,y}$	$I_{2,r}$
x_1	-1					
y_1		-1				
r_1		-L/2	-1			
x_2	1			-1		
y_2		1			-1	
r_2		-L/2	1		-L/2	-1
x_3				1		
y_3					1	
r_3					-L/2	1

Table 2-1 The contact situation of the system

From Table 2-1, the contact matrix **E** can be formulated:

$$\mathbf{E} = \begin{bmatrix} -1 & & & & & \\ & -1 & & & & \\ & -\frac{L}{2} & -1 & & & \\ 1 & & & -1 & & \\ & 1 & & & -1 & \\ & -\frac{L}{2} & 1 & & -\frac{L}{2} & -1 \\ & & & 1 & & \\ & & & & 1 & \\ & & & & -\frac{L}{2} & 1 \end{bmatrix} \tag{2-18}$$

Similarly, the formulation of the contact matrix can be generalized to any situation, including the discontinuous ice-structure contact. During the non-contact phase, any related entry in the contact matrix is replaced by zero. (See Subsection 3.4.1)

2.3.2 Inertia Matrix **M**

The inertia matrix is a block-diagonal matrix, which contains the information of elements' inertia. In two-dimensional coordinates, the information include the mass and the moment of inertia.

For the case of the above system, corresponding to each coordinate for each element, the inertia matrix can be easily formulated:

$$\mathbf{M} = \begin{bmatrix} m_1 & & & & & & & & \\ & m_1 & & & & & & & \\ & & I_{\mathrm{n},1} & & & & & & \\ & & & m_2 & & & & & \\ & & & & m_2 & & & & \\ & & & & & I_{\mathrm{n},2} & & & \\ & & & & & & m_3 & & \\ & & & & & & & m_3 & \\ & & & & & & & & I_{\mathrm{n},3} \end{bmatrix} \tag{2-19}$$

2.3.3 Compliance Matrix **T**

The compliant contact algorithm requires an additional term for the Lagrange multiplier formulation to solve, namely the compliance matrix, which is also a block-diagonal matrix. Each element of the matrix corresponds to the compliance factor for each contact constraint, see Equation (2-12).

For the case of the above system, the compliance matrix can be formulated as:

$$\mathbf{T} = \begin{bmatrix} CF_{1,x} & & & & & & \\ & CF_{1,y} & & & & & \\ & & CF_{1,r} & & & & \\ & & & CF_{2,x} & & & \\ & & & & CF_{2,y} & & \\ & & & & & CF_{2,r} \end{bmatrix} \tag{2-20}$$

2.3.4 Right-Hand-Side Vector **RHS**

According to the derivation of the compliant contact algorithm, the vector **RHS** contains the right-hand-side of the equation of the system, which reads:

$$\mathbf{RHS} = -\mathbf{K} \circ \left(\frac{\mathbf{1}}{\mathbf{4}} \mathbf{K} \Delta t + \frac{1}{2} \mathbf{C} \right)^{\circ -1} \circ \mathbf{u} - 2\dot{\mathbf{u}} \tag{2-21}$$

which can also be written as the equation below:

$$\mathbf{RHS} = -\mathbf{K} \circ \mathbf{CF} \cdot \Delta t \circ \mathbf{u} - 2\dot{\mathbf{u}} \tag{2-22}$$

where **CF** is the vector of compliance factors. Note that the displacement and velocity vectors are obtained from the previous time-loop, which include the influence of both implicit forces and explicit forces. (See Subsection 3.1.3)

2.3.5 Multiplier Vector **B**

The vector

$$\mathbf{B} = \begin{bmatrix} \Delta\dot{\mathbf{u}}_{im} \\ \boldsymbol{\lambda} \end{bmatrix}$$

is the multiplier that we sought for, which includes two different vectors. One is the velocity variation vector $\Delta\dot{\mathbf{u}}_{im}$, which indicates the velocity variation of elements caused by implicit forces in a time step. The other vector is the impulse vector $\boldsymbol{\lambda}$, which implies the impulse on each contact constraint.

When running the time-domain loop, the multiplier vector **B** is the crucial vector for iteration.

2.4 Catenary Mooring System

2.4.1 Introduction

The catenary mooring system is currently the most common type of mooring system employed in shallow water. The “catenary” refers to the shape of a free hanging line subjected to gravity. The catenary mooring system provides its anchoring structure with tension forces through the suspended weight and elastic properties of the mooring lines. In other words, the moored structure tends to lift the mooring lines under environmental loads, which creates tension forces.

In the catenary mooring system, the mooring lines terminate at the seabed horizontally, while the anchor points are only subjected to horizontal forces at the seabed. Thus, the mooring lines are required to be relatively long compared to the water depth. As the water depth increases, the weight and length of the mooring lines increase rapidly. A concept map of the catenary mooring system is shown in Figure 2-5.

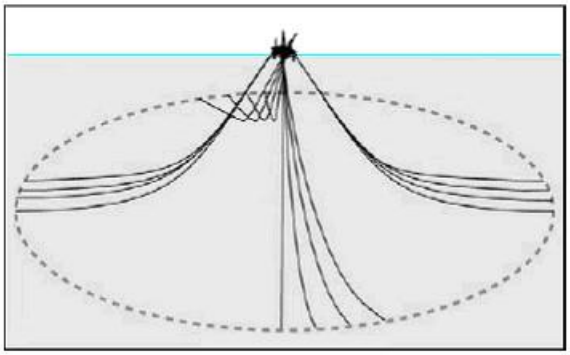

Figure 2-5 A concept map of the catenary mooring system

2.4.2 Catenary Equation

The catenary mooring system is built based on the catenary equation, which describes curves of strings subjected to gravitational loads. The catenary equation is widely used in various engineering fields for centuries. It has been developed in the last decades due to the need for anchoring floating structures. In the preliminary design, the static catenary method is commonly used to predict the anchoring situation, which is based on the following assumptions[8]:

1. The seabed is flat and horizontal;
2. Bending stiffness of the mooring line can be neglected;
3. The mooring lines are on a vertical plane comprising x-z coordinates only.

In the current study, the model of the mooring system is constructed analytically according to the catenary equation.

The equation of a catenary in Cartesian coordinates has the form

$$y = a\cosh\left(\frac{x}{a}\right) = \frac{a\left(e^{\frac{x}{a}} + e^{-\frac{x}{a}}\right)}{2} \tag{2-23}$$

where a is equivalent to a uniform scaling of the curve. Figure 2-6 illustrated catenary shapes for different values of a[9].

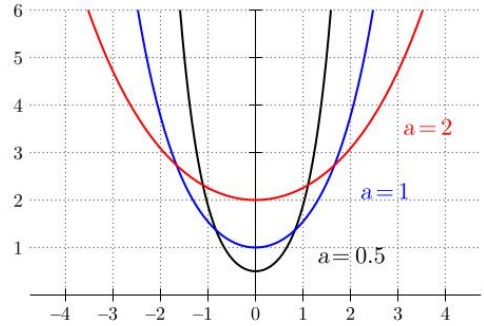

Figure 2-6 Catenary shapes for different values of a

While in terms of mooring catenary, a can be determined by the situation and the characteristics of the mooring line:

$$a = \frac{T_0}{g\lambda} \tag{2-24}$$

where T_0 is the horizontal component of tension at each point on the mooring line, g is the gravity acceleration, and λ is the linear density.

Based on the catenary equation, the shape of mooring line can be preliminarily determined. The derivation and determination of parameters of the mooring system are carried out in Chapter 4.

2.5 Conclusion

The basic theories supporting the process of the current model construction have been briefly presented in the chapter.

In conclusion, the compliant contact algorithm provides the solution for processing the elements' compliant contact under the frame of NDEM; the Lagrange multiplier formulation contributes the method of applying the algorithm to the model and solving for results; the catenary equation gives the method of preliminary design of the mooring line shape of the catenary mooring system.

3

NUMERICAL MODEL

This chapter provides a brief overview of the construction process of the numerical model. Overall, the numerical model is constructed according to the discrete element method (DEM), where the elements consist of the elements describing the level ice, and the structure is modeled as one element.

3.1 Model Overview

The numerical model is processed in the time domain. In each time loop, the result is calculated using the Lagrange multiplier formulation. Essentially, the behavior of the model is controlled by the velocity variation of elements in each time step. The velocity variation causes the displacement change, and thus one can observe the behavior of the model.

The velocity variation consists of two parts: the velocity variation caused by implicit forces and the velocity variation caused by explicit forces.

3.1.1 Implicit Forces

Implicit forces are the forces complying with the compliance contact algorithm. Thus, they can be processed by the Lagrange multiplier formulation implicitly. The values of implicit forces cannot be directly yielded by the formulation, however, its average value of a time step can be obtained by dividing the impulse by the length of a time step:

$$\mathbf{F}_{\text{im}} = \frac{\boldsymbol{\lambda}}{\Delta t} \tag{3-1}$$

The implicit forces act on the contact points and induce the velocity variation of the elements. The velocity variation caused by implicit forces can be obtained from Equation (2-15) or (2-16).

3.1.2 Explicit Forces

Explicit forces, on the other hand, are the forces not complying with the compliance contact algorithm. In the model, the explicit forces mainly include gravity, friction, and righting moments. Besides, while moving horizontally, the elements are subjected to the drag forces, which is counted as the explicit force as well.

The numerical model processes explicit forces by applying the acceleration vector. The equation reads as below:

$$\mathbf{a}_{\text{ex}} = \mathbf{F}_{\text{ex}} \circ \mathbf{m}^{\circ -1} \tag{3-2}$$

where $\mathbf{F}_{\text{ex}}$ is the vector of explicit forces, and $\mathbf{m}$ is the vector of inertia, which is also the diagonal vector of the inertia matrix (see Equation (2-19) for an example).

The vector of velocity variation due to explicit forces is formulated as below:

$$\Delta\dot{\mathbf{u}}_{\text{ex}} = \mathbf{a}_{\text{ex}} \cdot \Delta t \tag{3-3}$$

where Δt is the length of time step.

3.1.3 Time Loop Control

With both two parts of the velocity variation, the total velocity variation of the system can be formulated as below:

$$\Delta\dot{\mathbf{u}} = \Delta\dot{\mathbf{u}}_{\text{im}} + \Delta\dot{\mathbf{u}}_{\text{ex}} \tag{3-4}$$

As it is mentioned above, the velocity variation is the primary variable of the time loops, which controls the behavior of the model. Therefore, at the end of a time loop, the iteration of velocity and displacement are performed:

$$\dot{\mathbf{u}}^{(i+1)} = \dot{\mathbf{u}} + \Delta\dot{\mathbf{u}} \tag{3-5}$$

$$\mathbf{u}^{(i+1)} = \mathbf{u} + \dot{\mathbf{u}} \cdot \Delta t + \frac{1}{2}\Delta\dot{\mathbf{u}} \cdot \Delta t \tag{3-6}$$

The displacement and velocity vectors obtained at the end of a time loop will be applied into the Lagrange multiplier formulation (as entries of the right-hand-side vector) at the next time loop. In this way, the explicit forces will be able to influence the implicit forces, such that the implementation of a time loop is completed.

3.2 Level Ice Model

In the design condition, it is assumed that the sea level ice covers a large percentage of sea area, and thus, in the two-dimensional plane, the level ice has a considerable total length. In the numerical model, the level ice is divided into a large number of elements, where any physical properties of each element are identical. To simplify the problem, we consider the level ice as a homogeneous material. Thus, the gravitational load is distributed equally to each element, where the force-bearing point of each element is located at the center of gravity, which is also the geometric center of the element.

The current numerical model of the level ice is based on a two-dimensional plane which shows the side of the length-thickness of the level ice. However, it should be noted that the width of the level ice is also taken into account, which indicates that although the model is simulated two-dimensionally, it reflected the three-dimensional properties of objects. Subjected to gravity and buoyancy, the level ice has an initial draft. A typical model of the level ice is shown in Figure 3-1.

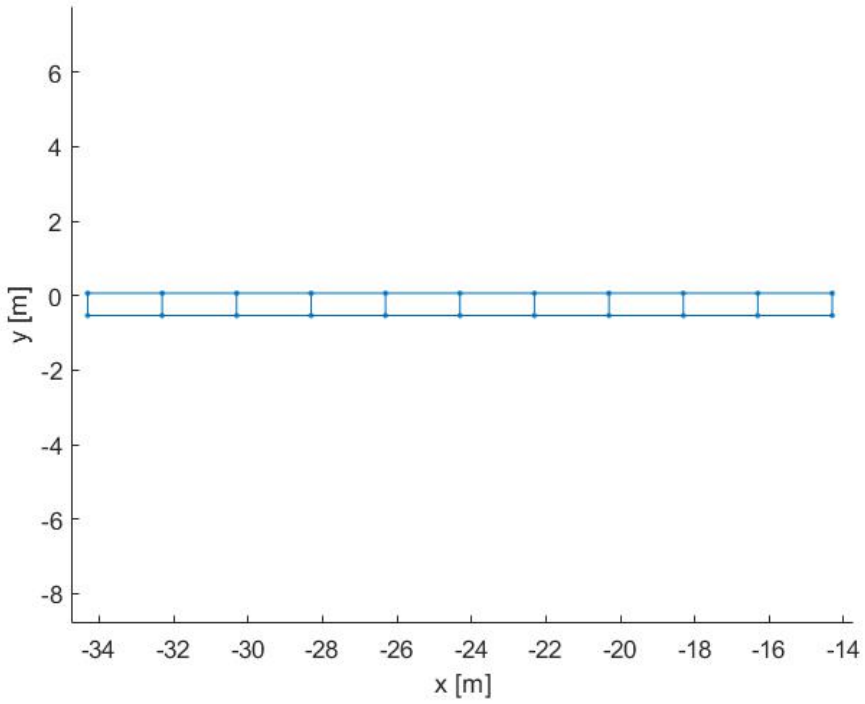

Figure 3-1 A typical level ice model in the two-dimensional plane

3.2.1 Ice-Ice Contact

As is mentioned in Chapter 2, when the level ice is not broken, the contact points between adjacent ice elements are considered fixed at the geometric center of the contact side, namely the side of the width-thickness. In the current study, the two ends of the level ice are set as free ends. Since each element has the same length l_i, the distance between centers of gravity of two adjacent elements equals to l_i as well. According to a paper by Yip et al., the contact stiffnesses in 3 degrees of freedom (normal, sheer and rotational) can be determined as below[10]:

$$k_{n,i} = \frac{E_i A_i}{l_i}, \quad k_{t,i} = \frac{G_i A_i}{l_i}, \quad k_{r,i} = \frac{E_i I_{t,i}}{l_i} \tag{3-7}$$

where E_i and G_i are Young's modulus and the shear modulus of level ice, respectively, while A_i is the side sectional area of the level ice, and $I_{t,i}$ is the second moment of area.

The contact damping coefficients can be set proportional to the corresponding stiffnesses, according to the paper by Vliet et al[11]. However, there is no any reference found regarding the specific determination of damping values, therefore, the thesis currently sets the damping values as 10% of the ice element's corresponding critical damping values.

3.2.2 Buoyancy

To simulate the buoyancy, we can assume the level ice connected to an elastic foundation, thus the buoyancy is set as an implicit force, the equivalent stiffness can be formulated as below:

$$k_{\mathrm{b,i}} = \rho_{\mathrm{w}} g b_{\mathrm{i}} l_{\mathrm{i}} \tag{3-8}$$

where ρ_{w} is the density of sea water, g is the gravity acceleration; b_{i} and l_{i} are the width and the element length of the level ice, respectively.

Similarly, the damping coefficient of buoyancy can also be set proportional to the stiffness.

3.2.3 Lagrange Multiplier Formulation

To process the implicit forces on the level ice model including the above ice-ice contact force and the buoyancy, we apply the Lagrange multiplier formulation.

Figure 3-2 depicts a schematic diagram of contacts in the level ice model, where the dots indicate the contact constraints in the level ice model. The red dots between adjacent elements indicate the ice-ice contact, each of which includes three contact constraints; the yellow dots beneath the elements indicate the buoyancy, each counts for one contact constraint.

Figure 3-2 A schematic diagram of contacts in the level ice model

Therefore, for a level ice model with an element number of N_{i}, the total number of contact constraints is:

$$n_{\mathrm{c,i}} = 3 \cdot \left(N_{\mathrm{i}} - 1\right) + N_{\mathrm{i}} = 4N_{\mathrm{i}} - 3 \tag{3-9}$$

The total number of degrees of freedom in the model, on the other hands, is three times the element number:

$$n_{\mathrm{dof,i}} = 3N_{\mathrm{i}} \tag{3-10}$$

Similar to the derivation in Section 2.3, we can derive the required matrices according to the above information.

For the level ice with element length l_{i}, the contact matrix $\mathbf{E}_{\mathrm{i}}$ has $(3n)$ rows and $(4n\text{-}3)$ columns:

$$\mathbf{E}_{\mathrm{i}}=\begin{bmatrix}
-1 & & & & & & & \cdots & & & \\
1 & & -1 & & & & & \cdots & & & \\
 & & -l_{\mathrm{i}}/2 & -1 & & & & \cdots & & & \\
 & 1 & & & & -1 & & \cdots & & & \\
 & & 1 & & 1 & & -1 & \cdots & & & \\
 & & -l_{\mathrm{i}}/2 & 1 & & & -l_{\mathrm{i}}/2 & -1 & \cdots & & & \\
\vdots & \vdots & \vdots & \vdots & \vdots & \vdots & \vdots & \vdots & \ddots & & & \\
 & & & & & & & & & 1 & & \\
 & & & & & & & & & & 1 & 1 \\
 & & & & & & & & & -l_{\mathrm{i}}/2 & 1 &
\end{bmatrix} \tag{3-11}$$

The inertia matrix $\mathbf{M}_{\mathrm{i}}$ has ($3n$) diagonal elements:

$$\mathbf{M}_{\mathrm{i}}=\begin{bmatrix}
m_1 & & & & & & & & & & \\
 & m_1 & & & & & & & & & \\
 & & I_{\mathrm{n},1} & & & & & & & & \\
 & & & m_2 & & & & & & & \\
 & & & & m_2 & & & & & & \\
 & & & & & I_{\mathrm{n},2} & & & & & \\
 & & & & & & \ddots & & & & \\
 & & & & & & & m_n & & & \\
 & & & & & & & & m_n & & \\
 & & & & & & & & & I_{\mathrm{n},n} &
\end{bmatrix} \tag{3-12}$$

The compliance matrix $\mathbf{T}_{\mathrm{i}}$ has ($4n$-3) diagonal elements:

$$\mathbf{T}_{\mathrm{i}}=\begin{bmatrix}
CF_{\mathrm{b},1} & & & & & & & & & & \\
 & CF_{\mathrm{l},x} & & & & & & & & & \\
 & & CF_{\mathrm{l},y} & & & & & & & & \\
 & & & CF_{\mathrm{l},r} & & & & & & & \\
 & & & & CF_{\mathrm{b},2} & & & & & & \\
 & & & & & CF_{2,x} & & & & & \\
 & & & & & & CF_{2,y} & & & & \\
 & & & & & & & CF_{2,r} & & & \\
 & & & & & & & & \ddots & & \\
 & & & & & & & & & CF_{n-1,x} & \\
 & & & & & & & & & & CF_{n-1,y} \\
 & & & & & & & & & & & CF_{n-1,r} \\
 & & & & & & & & & & & & CF_{\mathrm{b},n}
\end{bmatrix} \tag{3-13}$$

Correspondingly, the vectors $\mathbf{RHS}_{\mathrm{i}}$ and $\mathbf{B}_{\mathrm{i}}$ can be easily formulated.

3.2.4 Drag Force

When the level ice moves horizontally on the sea water, it is subjected to the drag force due to the viscosity of sea water. In the model, the drag force due to the viscosity of air is too small, so it can be neglected. The drag we discuss here refers to the profile drag, which is the sum of form drag and skin friction drag:

$$F_{\mathrm{D,i}} = F_{\mathrm{D,f,i}} + F_{\mathrm{D,s,i}} \tag{3-14}$$

The form drag force exists at the side edge of the level ice, which can be obtained by the following equation:

$$F_{\mathrm{D,f,i}} = -\frac{1}{2}\rho_{\mathrm{w}} c_{\mathrm{d,f,i}} b_{\mathrm{i}} d_{\mathrm{i}} \dot{u}_{\mathrm{i}} \left|\dot{u}_{\mathrm{i}}\right| \tag{3-15}$$

where $c_{\mathrm{d,f,i}}$ is the form drag coefficient of the level ice, b_{i} the width of the level ice, and d_{i} is the draft of the level ice. As it can be seen from the equation, the value of form drag force is proportional to the square of the velocity, and its direction is contrary to the direction of velocity.

The skin friction drag force exists at the bottom of the level ice, the interface between the level ice and sea water. The skin friction drag force of an ice element can be obtained by the following equation:

$$F_{\mathrm{D,s,i}} = -\frac{1}{2}\rho_{\mathrm{w}} c_{\mathrm{d,s,i}} b_{\mathrm{i}} l_{\mathrm{i}} \dot{u}_{\mathrm{i}} \left|\dot{u}_{\mathrm{i}}\right| \tag{3-16}$$

where $c_{\mathrm{d,s,i}}$ is the skin friction coefficient of the level ice. As it can be seen from the equation, the value of skin friction drag force is proportional to the square of the velocity, and its direction is contrary to the direction of velocity.

In the numerical model, the drag force of level ice is considered as an explicit force. Further, the drag coefficients will be determined in Chapter 4.

3.3 Moored Structure Model

The moored structure model consists of two parts: the buoy structure and the catenary mooring system. The buoy structure is modeled as a rigid body, while the mooring lines are modeled analytically according to the catenary equation.

Subjected to gravity and buoyancy, the buoy has an initial draft as well.

3.3.1 Buoyancy & Hydrostatic Stability

Generally, the buoyancy provides the buoy with both the vertical and rotational equilibrium. To simulate the buoyancy of the buoy structure, we can first assume an elastic spring connected at the center point of the bottom keel of the buoy; the equivalent stiffness can be formulated as below:

$$k_{\mathrm{b,s}} = \rho_{\mathrm{w}} g \pi \left(\frac{D_{\mathrm{s,wl}}}{2}\right)^2 \tag{3-17}$$

where ρ_w is the density of sea water, g is the gravity acceleration, and $D_{s,wl}$ is the waterline diameter of the buoy.

Similarly, the damping coefficient of buoyancy can also be set proportional to the stiffness. By this approach, the buoyancy is considered as an implicit force.

However, by the method applied above, the buoyancy only provides the buoy structure with vertical equilibrium, which is not sufficient to simulate the whole effect of the buoyancy. Furthermore, the buoyancy should be able to provide the rotational equilibrium to satisfy the hydrostatic stability, which is implemented by applying righting moments. Specifically, if one adds an (external) heeling moment M_H to a structure, it will heel with an angle. An equilibrium will be achieved when the righting moments M_S equals the heeling moment M_H; see Figure 3-4.

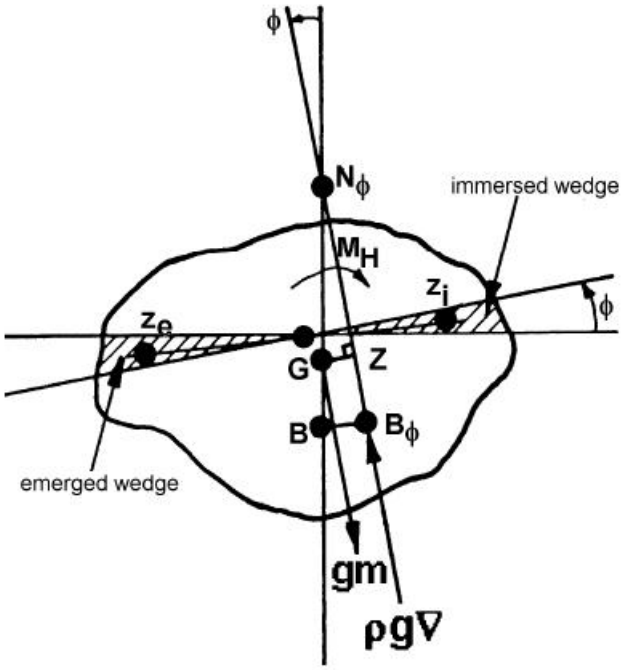

Figure 3-4 Rotation Equilibrium at an angle of heel[12]

The righting moment induced by the hydrostatic stability is written as:

$$M_S = \rho_w g \nabla \cdot \overline{GN_\phi} \cdot \sin\phi \tag{3-18}$$

where $\overline{GN_\phi}$ can be obtained by:

$$\overline{GN_\phi} = \overline{KB} + \frac{I_T}{\nabla} \cdot \left(1 + \frac{1}{2}\tan^2\phi\right) - \overline{KG} \tag{3-19}$$

Here, K is the keel point of the structure, B is the center of buoyancy, and G is the center of gravity. I_T is the second moment of area of the water plane, and ∇ is the displacement volume.

Noted that the righting moment here is applied as an explicit force into the model.

3.3.2 Mooring System

The mooring system in the two-dimensional plane consists of two mooring lines with their upper ends attached to the structure at the positions of fairleads and their lower ends anchored at the seabed.

The mooring system provides its anchoring structure with horizontal equilibrium and a part of rotational equilibrium. To be more specific, the difference of forces applied to the mooring lines at the fairlead implement the equilibrium. To investigate the effects in different direction, we can first orthogonally decompose the force. The total horizontal force is as known as the restoring force:

$$F_{\mathrm{R}} = F_{x1} + F_{x2} \tag{3-20}$$

Previous researches have concluded the dynamic behaviors of the mooring system, and a brief conclusion is demonstrated below. Figure 3-5 shows an example of results of static catenary line calculations for a moored structure. Figure 3-5.a shows the structure anchored by two mooring lines of chain at 100 m water depth. Figure 3-5.b shows the horizontal forces at the suspension points of both mooring lines as a function of the horizontal displacement of the platform. Finally, figure 3-5.c shows the relation between the total horizontal force on the structure and its horizontal displacement. This figure shows clearly the non-linear relation between the horizontal force on the moored structure and its horizontal displacement.

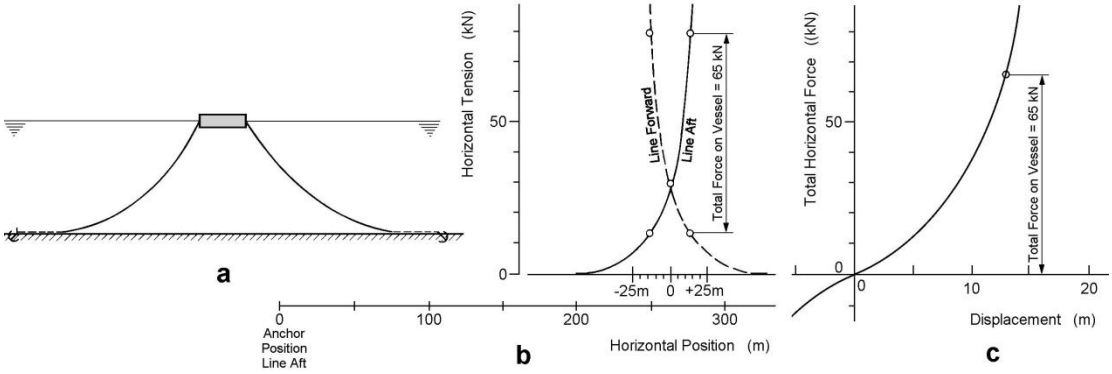

Figure 3-5 Horizontal forces on a moored structure as a function of its horizontal displacement[13]

To process the above non-linear relation, we can divide the restoring force into two components: the linear component and the non-linear component, see Figure 3-6.

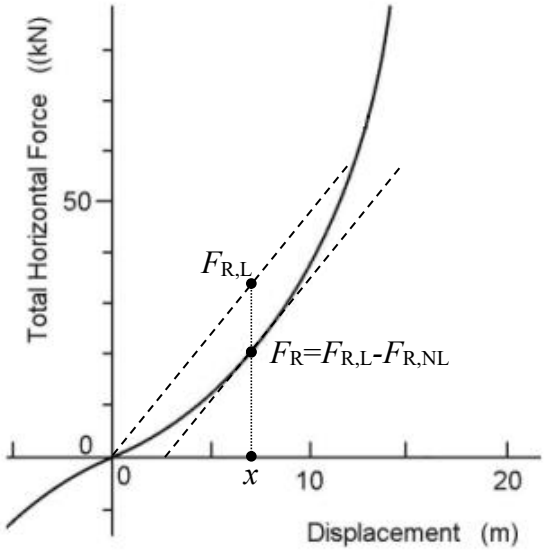

Figure 3-6 The non-linear relation between the total horizontal force and the displacement

For a specific horizontal displacement x, the corresponding restoring force is F_r. From the tangent slope of the curve, we can obtain the equivalent stiffness of the linear component k_R, and thus the linear component can be obtained:

$$F_{R,L} = k_R \cdot x \tag{3-21}$$

With the equivalent stiffness, the linear component can be considered as an implicit force, and processed by the Lagrange multiplier formulation.

Correspondingly, the non-linear component is considered as an explicit force, which is written as:

$$F_{R,NL} = F_{R,L} - F_R \tag{3-22}$$

Besides, due to the weight of mooring lines, the moored structure is also subjected to a vertical downward pull force, which is an explicit force:

$$F_{m,y} = -\left(F_{y1} + F_{y2}\right) \tag{3-23}$$

Furthermore, the mooring system provides the buoy structure with righting moment in case of inclination. The righting moment induced by the mooring system is obtained as:

$$M_m = -F_{x1}\overline{y_1} - F_{x2}\overline{y_2} + F_{y1}\overline{x_1} - F_{y2}\overline{x_2} \tag{3-24}$$

where $\overline{x}$ is the horizontal distance between the fairlead and the center of gravity, while $\overline{y}$ is the vertical distance between the fairlead and the center of gravity. The subscripts indicate the numbering of the fairlead.

Together with the righting moment induced by the hydrostatic stability in Equation (3-18), the total righting moment of the moored structure can be obtained:

$$M_R = M_S + M_m \tag{3-25}$$

3.3.3 Drag Force

Similarly to the drag force of level ice, when the moored structure moves horizontally on the sea water, it is subjected to the drag force as well due to the viscosity of sea water. The drag we discuss here refers to the profile drag, which is the sum of form drag and skin friction drag:

$$F_{\mathrm{D,s}} = F_{\mathrm{D,f,s}} + F_{\mathrm{D,s,s}} \tag{3-26}$$

The form drag force of the structure can be obtained by the following equation:

$$F_{\mathrm{D,f,s}} = -\frac{1}{2}\rho_{\mathrm{w}} c_{\mathrm{d,f,s}} A_{\mathrm{s}} \dot{u}_{\mathrm{s}} \left|\dot{u}_{\mathrm{s}}\right| \tag{3-27}$$

where $c_{\mathrm{d,f,s}}$ is the form drag coefficient of the structure, and A_{s} is the side sectional area of the structure under the waterline. As it can be seen from the equation, the value of form drag force is proportional to the square of the velocity, and its direction is contrary to the direction of velocity.

The skin friction drag force exists at the bottom of the structure, the interface between the structure and sea water. The skin friction drag force of the structure can be obtained by the following equation:

$$F_{\mathrm{D,s,s}} = -\frac{1}{2}\rho_{\mathrm{w}} c_{\mathrm{d,s,s}} A_{\mathrm{b}} \dot{u}_{\mathrm{i}} \left|\dot{u}_{\mathrm{i}}\right| \tag{3-28}$$

where $c_{\mathrm{d,s,s}}$ is the skin friction coefficient of the structure, and A_{b} is the bottom sectional area of the structure under the waterline. As it can be seen from the equation, the value of skin friction drag force is proportional to the square of the velocity, and its direction is contrary to the direction of velocity.

In the numerical model, the drag force on the structure is considered as an explicit force. Further, the drag coefficients will be determined in Chapter 4.

3.4 Ice-Structure Interaction

With both the level ice and moored structure models accomplished, we can now investigate the ice-structure interaction.

During the simulation, the right end of the level ice will contact with the moored structure. Generally, the following processes can happen simultaneously during the interaction:

1. Ice compressive failure: The level ice fractures at the position of the contact point due to compression;
2. Ice bending failure: The level ice breaks at a specific length due to bending moment;
3. Friction: The ice slides along the structure hull, exerting a frictional force.

3.4.1 Ice Compressive Failure

Due to the relatively low compressive strength of the ice, the level ice fractures at the position of the contact point under compression during the contact.

Figure 3-7 shows the diagram of the ice-structure contact, where δ is the overlapping distance (also known as the penetration), α the downward-sloping hull angle of the structure, β the angle between the structure's downward-sloping hull and the level ice (also known as the contact angle), and a is the contact area.

The contact points both on the level ice and the structure are shown as solid dots in Figure 3-7. In reality, the overlapping distance δ is always relatively small, therefore, to simplify the problem, we can assume the relative position of the contact point on the level ice remains unchanged at the upper-right edge, and the contact point on the structure is the point where a line perpendicular to the structure hull and through the ice contact point crosses the hull. During the contact, the relative position of the contact point on the structure can change over time.

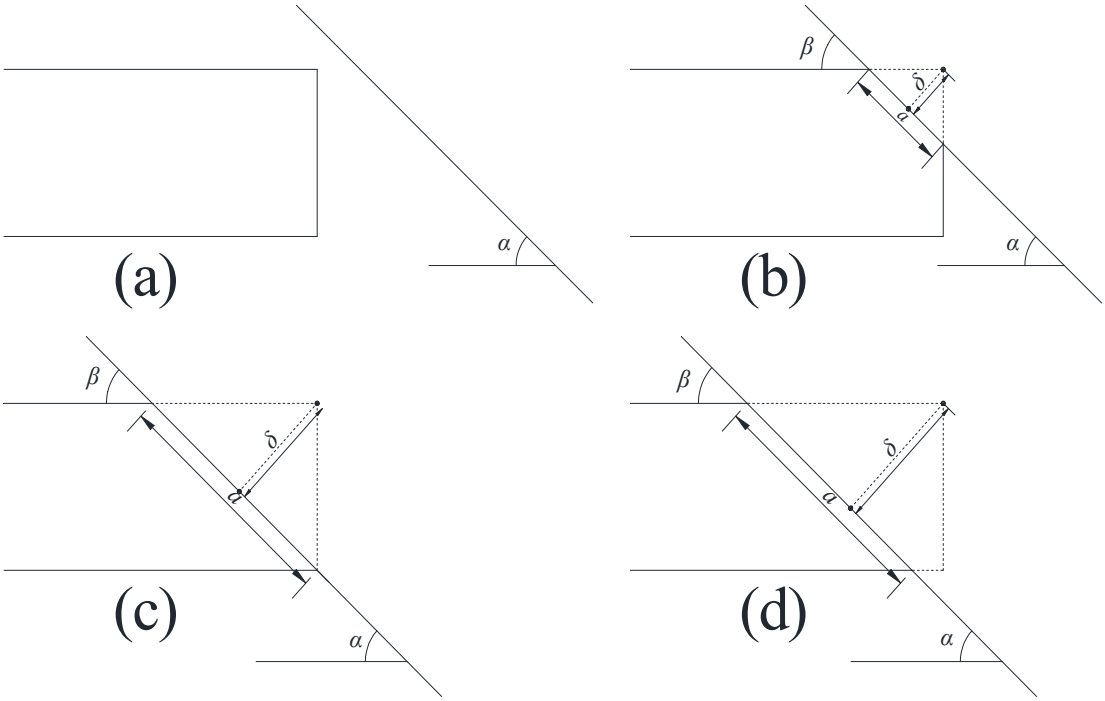

Figure 3-7 The ice-structure contact diagram

Generally, the contact can be summarized in 3 phases:

No-contact Phase

In this phase (Figure 3-7.a), the structure does not contact with the level ice. Therefore, there is no interaction between them. The vector entry of the ice-structure contact in the overall contact matrix in this phase is a zero vector:

$$\mathbf{E}_c = [0 \quad 0 \quad 0 \quad 0 \quad 0 \quad 0]^T \tag{3-29}$$

Contact Phase

In this phase (Figure 3-7.b), the structure is contacting with the level ice. There is an interaction between the structure and the level ice. Due to the relatively low compressive strength of ice, the overlapping part of level ice will crush into crushed ice. The vector entry of the ice-structure contact in the overall contact matrix in this phase is:

$$\mathbf{E}_c = \begin{bmatrix} -\sin\beta & -\cos\beta & 0 & \sin\beta & \cos\beta & 0 \end{bmatrix}^T \tag{3-30}$$

Over-contact Phase

Once the contact area a reached the maximum (Figure 3-7.c), even if the penetration δ increases (Figure 3-7.d), the interaction between the structure and the level ice will remain unchanged.

However in reality, when the ice contacts with the structure's downward-sloping hull, due to bending and other mechanisms, the over-contact phase of the ice is rarely observed. Therefore, we will only focus on the non-contact phase and the contact phase. The influence of crushed ice is relatively too small to be taken into account as well, considering that the size of the crushed ice due to compressive failure is tiny.

The contact between the level ice and the structure is considered as the compliant contact. To accurately identify the phase of the ice-structure interaction, a criterion regarding two contact points[i] is applied. If the following inequality is satisfied, the system is under the contact phase, otherwise it is under the non-contact phase.

$$\dot{u}_r \cdot \Delta t > -d_r + \delta_{max} \tag{3-31}$$

where $\dot{u}_r$ is the relative velocity of two contact points[ii], d_r the relative distance between two contact points[iii], while δ_{max} is the maximum penetration, taking the size loss of the level ice into account. To be more specific, the positive directions of the relative velocity and the relative distance are shown in Figure 3-8.(a) and 3-8.(b), respectively.

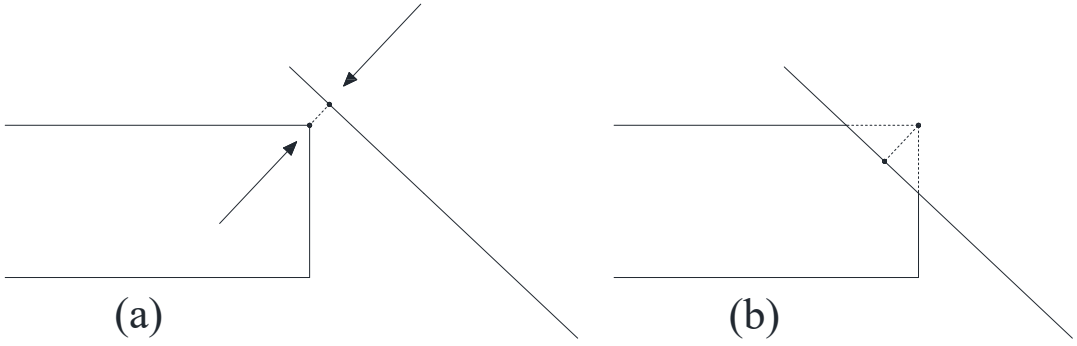

Figure 3-8 The positive directions of the relative velocity (a) and the relative distance (b)

The above criterion measures the relationship between the relative displacement of the two contact points in one time-step and the relative distance of the two contact points.

[i] One on the level ice and another on the structure's surface.
[ii] Positive values imply the direction that the penetration has an increasing tendency.
[iii] Positive values indicate that the two models are overlapping.

To simulate the contact in the model, we need to first determine the contact stiffness. The contact force between the level ice and the structure can be obtained as below:

$$F_c = A_c \cdot \sigma_{c,i} \tag{3-32}$$

where A_c is the contact area, and σ_c is the compressive strength of the ice.

The contact area is related to the penetration δ:

$$A_c = \frac{\delta \cdot b_i}{\sin\beta \cdot \cos\beta} \tag{3-33}$$

where b_i is the width of the level ice.

In this way, we can calculate the contact stiffness:

$$k_c = \frac{F_c}{\delta} = \frac{\delta \cdot b_i \cdot \sigma_{c,i}}{\delta \cdot \sin\beta \cdot \cos\beta} = \frac{b_i \cdot \sigma_{c,i}}{\sin\beta \cdot \cos\beta} \tag{3-34}$$

Thus, the contact stiffness is written as:

$$k_c = \frac{b_i \cdot \sigma_{c,i}}{\sin\beta \cdot \cos\beta}, \quad 0 < \beta < \frac{\pi}{2} \tag{3-35}$$

With the stiffness coefficient determined, the constraint matrices **E** for both the contact phase and the no-contact phase can be set up for the Lagrange multiplier formulation.

The ice-structure contact is considered associated with several mechanisms, which include but not limited to the contact stiffness, the normal contact force, and the contact impulse. Therefore, to ensure the contact model works correctly, the following necessary conditions are needed to be satisfied:

(1) The contact stiffness should be higher than or equal to zero;
(2) At the beginning of a time-step, the normal contact force should be higher than or equal to zero;
(3) The contact force exists only when the penetration is larger than or equal to zero;
(4) The contact impulse should not be negative;
(5) The contact impulse should be smaller than or equal to the contact impulse needed to make the relative contact velocity zero.

The contact stiffness has been determined in Equation (3-35). The value of the contact stiffness will always be positive given that the contact angle β is smaller than $\frac{\pi}{2}$. Therefore, the condition (1) is satisfied.

Further, to satisfy the conditions (2)-(5), the output of impulse at the contact area should be restricted. Therefore, the Gauss-Seidel method is additionally applied here to solve the Lagrange multiplier formulation here. To apply the Gauss-Seidel method, we need to first define the dominant matrix **A**, which is from Equation (2-16):

$$\mathbf{A} = \mathbf{E}^{\mathrm{T}}\mathbf{M}^{-1}\mathbf{E} + \mathbf{T} \tag{3-36}$$

Thus, the basic formula for the Gauss-Seidel iteration is written as below:

$$\boldsymbol{\lambda}_i^{(k+1)} = \frac{1}{\mathbf{A}_{ii}}\left(\mathbf{RHS}_i - \sum_{j<i} \mathbf{A}_{ij}\boldsymbol{\lambda}_j^{(k+1)} - \sum_{j>i} \mathbf{A}_{ij}\boldsymbol{\lambda}_j^{(k)} \right), \quad i, j = 1,2,...,n \tag{3-37}$$

where $\boldsymbol{\lambda}$ is the impulse vector we sought for, $\mathbf{A}$ the dominant matrix, and **RHS** is the right-hand-side vector. *k* here stands for the arbitrary step of iterations.

There are two primary limitations for the output of contact impulse needed to be embedded into the Gauss-Seidel iteration, namely to satisfy the conditions (4) and (5).

The first limitation is known as the **"Non-negativity limitation"**, which means the contact impulse should not be negative:

$$\lambda_{\mathrm{c}} \geq 0 \tag{3-38}$$

The second limitation is known as the **"Maximum impulse limitation"**, namely to limit the contact impulse to be smaller than or equal to the contact impulse needed to make the relative contact velocity zero:

$$\lambda_{\mathrm{c}} \leq \lambda_{\mathrm{c,max}} \tag{3-39}$$

This is calculated with the dominant matrix that is derived without compliance factors, which is denoted as $\mathbf{A_0}$:

$$\mathbf{A_0} = \mathbf{E}^{\mathrm{T}}\mathbf{M}^{-1}\mathbf{E} \tag{3-40}$$

The maximum contact impulse is thus calculated within the iteration as below:

$$\lambda_{\mathrm{c,max}}^{(k+1)} = \frac{1}{\mathbf{A}_{\mathbf{0},cc}}\left(\dot{u}_{\mathrm{r}} - \mathbf{A}_{\mathbf{0},c}\boldsymbol{\lambda}^{(k)} + \mathbf{A}_{\mathbf{0},cc}\boldsymbol{\lambda}_c^{(k+1)} \right) \tag{3-41}$$

where *c* is the numbering represented for the location of ice-structure contact.

The average contact normal force can thus be obtained by dividing the impulse with time step:

$$F_{\mathrm{c}} = \frac{\lambda_{\mathrm{c}}}{\Delta t} \tag{3-42}$$

3.4.2 Ice Bending Failure

The interaction between the level ice and the structure's downward-sloping hull can cause ice bending failure due to high bending moment. Specifically, during the simulation, the level ice moves towards the structure with a certain velocity; at a particular moment, when the level ice contacts with the structure's downward-sloping hull at the position of the contact point, the level ice generates a bending moment along the direction of length. If the flexural stress of the level ice at some position exceeds its flexural strength, the bending failure occurs. The level ice will fracture at this position and produce crushed ice, while the rest of the level ice will continue to move towards the structure. In reality, the crushed ice interact with the structure as

well, however, in the current study, we do not focus on the crushed ice, therefore in this thesis, the influence of the crushed ice will be ignored.

For each time-step, the bending moment of the level ice at each contact point can be obtained. By summarizing each value along the length, one can plot a curve of the overall bending moment of the level ice. The derivation of bending moments in the model are given as below.

Although the ice bending occurs mainly due to the force in the vertical direction, namely the shear force applied to the level ice, the horizontal forces also induce the bending moment as a result of deflections along the level ice. Therefore, it will be not sufficiently accurate to calculate the bending moment only based on the vertical force. Alternatively, bending moments can be obtained based on the rotation of each ice element. The bending moment at the location of x equals to the ice-ice rotational stiffness multiplied by the relative rotation of its adjacent elements:

$$M_{\mathrm{b}}(x) = k_{\mathrm{r,i}} \cdot r(x) \tag{3-43}$$

With the bending moment, one can calculate the flexural stress as below:

$$f_{\mathrm{b}}(x) = \frac{M_{\mathrm{b}}(x) t_{\mathrm{i}}}{2 I_{\mathrm{t,i}}} \tag{3-44}$$

When the flexural stress at a specific length exceeds the ice flexural strength, the bending failure occurs, where the specific length is known as the breaking length. The breaking length is primarily related to the relative velocity between the level ice and the structure. The detailed result of the relation and its verification will be discussed in Chapter 5.

In the model, the bending failure manifests as the cancellation of the fixed connection at the failure occurring contact point. Since we do not focus on the crushed ice, the broken part will no longer appear in the remaining time of the simulation.

3.4.3 Friction

The contact between the level ice and the structure also induces the friction due to the relative motion of solid surfaces. Although the friction includes both the static friction and the dynamic friction, in reality, the static friction in the ice-structure interaction is rarely observed. Therefore, we only focus on the dynamic friction in the model.

The dynamic friction can be obtained with the normal force at the contact point:

$$F_{\mathrm{f}} = \mu \cdot F_{\mathrm{c}} \tag{3-45}$$

where μ is the friction coefficient. A recommended value for this coefficient is around 0.1, according to a guidance from Bureau Veritas[14].

The direction of the friction is perpendicular to the normal force and opposite to the direction of the relative movement of two surfaces.

3.5 Conclusion

This chapter provides a thorough description of the model construction process. In summary, the model consists of the level ice model and the moored structure model. To process the interactions inside and between these models, including the ice-ice contact and the ice-structure interaction, the model distinguishes two different types of forces, namely the implicit forces and the explicit forces. The implicit forces are processed by the Lagrange multiplier formulation, while the explicit forces are processed by applying the acceleration vectors in the time-loop control.

4

MODEL PARAMETER DETERMINATIONS

This chapter carries out a series of parameter determinations for the primary objects in the model, including the level ice, the buoy structure, and the mooring system. With reasonable parameters applied in the model, the results of the simulation will be more realistic, and more accurate as well.

4.1 Level Ice

Most of the parameters of level ice are significantly associated with the geographic location of the model. As mentioned in Chapter 1, the model is assumed set up at a leeward of the Svalbard Archipelago, where only the first-year ice is considered. In this section, all necessary parameters of the level ice will be determined.

4.1.1 Size Parameters

The size parameters of level ice include: total length, element length, thickness, and width.

The total length of level ice mainly influences the momentum of the ice sheet in the ice-structure interaction. To ensure the viability of the numerical simulation, the level ice is required to have sufficient total length for bending failure to occur. Since in the Arctic environment, the entire sea area is considered covered by ice, there is no upper limit for the total length of the level ice. In order to satisfy a sufficient momentum, as well as to keep the accuracy and processing speed reasonable, only a finite length segment of the level ice adjacent to the ice-structure contact is discretized, so that the level ice model is in fact divided into two parts: discretized ice elements, and the un-discretized ice. The discretized ice elements are the primary objects of the investigation, while the un-discretized ice is mainly applied to provide the level ice with sufficient momentum, which can be treated as one element and usually located far away from the ice-structure contact.

Generally, the number of discretized ice elements is a primary factor influencing the overall accuracy of the simulation results. Theoretically, the larger the number of discretized ice elements is, the more accurate the result will be. However, due to the limitation of processing speed, the number of discretized ice elements is limited as well.

As far as the width is concerned, one can not determine the width of the level ice without considering the actual contact area of ice-structure interaction. The level ice

model has a so-called "effective width", which is identical with the width of the ice-structure contact area, roughly the waterline width of the structure.

Furthermore, in consultation with experts on the ice condition around the Svalbard Archipelago, the thickness of the level ice is chosen as 0.6 m. Therefore, together with the effective width, the area of the contact surface between two adjacent ice element can be determined:

$$A_{\mathrm{i}} = b_{\mathrm{i}} \cdot t_{\mathrm{i}} \tag{4-1}$$

4.1.2 Density

The density of the pure ice at 0 ℃ is 916.8 kg/m^3. However, the density of the sea ice can be smaller due to salinity and porosity. Here, we choose the average density of the sea ice as the density applied to our level ice model:

$$\rho_{\mathrm{i}} = 910\ \mathrm{kg/m^3} \tag{4-2}$$

4.1.3 Rotational Properties

When dealing with the rotational motion, which is around the axis of the width direction, two essential values are needed to be calculated first. One is the moment of inertia:

$$I_{\mathrm{n,i}} = \frac{m_{\mathrm{i}}\left(l_{\mathrm{i}}^2 + t_{\mathrm{i}}^2\right)}{12} \tag{4-3}$$

The other one is the second moment of area:

$$I_{\mathrm{t,i}} = \frac{b_{\mathrm{i}} t_{\mathrm{i}}^3}{12} \tag{4-4}$$

4.1.4 Young's Modulus & Shear Modulus

The Young's modulus and the shear modulus of the sea ice are two parameters required to process the deformation of the level ice. The values of Young's modulus range from approximately 2 GPa at low-frequency loading to a high-frequency value of 9 GPa, according to *Ice Engineering*[15]. Here we can just take a relatively average value:

$$E_{\mathrm{i}} = 5.0\ \mathrm{GPa} \tag{4-5}$$

The Poisson's ratio for sea ice ν_{i} is taken as 0.3, therefore, the shear modulus can be obtained as below:

$$G_{\mathrm{i}} = \frac{E_{\mathrm{i}}}{2\left(1+\nu_{\mathrm{i}}\right)} = 1.9\ \mathrm{GPa} \tag{4-6}$$

With these modulus obtained, the ice-ice contact stiffness can be calculated according to Equation (3-7).

4.1.5 Compressive Strength

Values of the uniaxial compressive strength for ice range from 0.5 to 20 MPa, according to *Ice Engineering*. The strength is a function of strain rate, temperature, grain size, grain structure, and porosity. According to the guidance from Bureau Veritas, values range from 1.5 to 5 MPa in most parts of the Arctic region. As for the sea ice in the region of the Svalbard Archipelago, the compressive strength can be taken as:

$$\sigma_{c,i} = 3.0 \text{ MPa} \tag{4-7}$$

4.1.6 Flexural Strength

The flexural strength is required when dealing with the ice bending failure. The following are the determination process of the ice flexural strength from *ISO19906*[16]:

Firstly, the salinity of the sea ice (in ‰) is required:

$$\begin{cases} S_i = 13.4 - 17.4 t_i & \text{for } t_i \le 0.34 \text{ m} \\ S_i = 8.0 - 1.62 t_i & \text{for } t_i \ge 0.34 \text{ m} \end{cases} \tag{4-8}$$

where t_i is the ice thickness. This approach implies that there is no salinity variation with depth.

With the salinity obtained, the brine volume fraction (in ‰) can be determined by:

$$v_{b,i} = S_i \left(\frac{49.18}{|T_i|} + 0.53 \right) \tag{4-9}$$

where T_i is the average ice temperature, in ℃.

Finally, the flexural strength (in MPa) can be determined by:

$$\sigma_{f,i} = 1.76 e^{-5.88\sqrt{v_{b,i}}} \tag{4-10}$$

The average temperature of the sea ice at the Svalbard Archipelago can be assumed as -10 ℃ according to related experts, therefore, the flexural strength of the sea ice in this region can be calculated, the result is:

$$\sigma_{f,i} = 0.56 \text{ MPa} \tag{4-11}$$

4.1.7 Drag Coefficient

As mentioned in Chapter 3, the drag we discuss here is known as the profile drag, which includes the form drag and the skin friction drag, where they both have a drag coefficient, respectively.

The form drag coefficient for the level ice can be assumed according to Horner[17]:

$$c_{\mathrm{d,f,i}} = 1.0 \tag{4-12}$$

The skin friction drag coefficient for the level ice, on the other hand, is related to the Reynolds number of the flow. Since the speed of flow in the Arctic region is considered relatively low, thus the flow can be assumed as a Laminar flow. In the Laminar flow, the skin friction drag coefficient is obtained according to Blasius solution[18]:

$$c_{\mathrm{d,s,i}} = \frac{0.664}{\sqrt{\mathrm{Re_i}}} \tag{4-13}$$

where

$$\mathrm{Re_i} = \frac{\rho_{\mathrm{w}} \dot{u} x}{\mu_{\mathrm{w}}} \tag{4-14}$$

which is the Reynolds number, and x is the distance from the reference point at which a boundary layer starts to form (the edge of the level ice), while μ_{w} is the dynamic viscosity of the sea water.

4.1.8 Summary

The values of the main parameters about the level ice elements are concluded in Table 4-1.

Effective width	b_{i}	8.48	m
Thickness	t_{i}	0.6	m
Contact surface area	A_{i}	5.09	$\mathrm{m^2}$
Density of sea ice	ρ_{i}	910	$\mathrm{kg/m^3}$
Density of sea water	ρ_{w}	1025	$\mathrm{kg/m^3}$
Moment of inertia	$I_{\mathrm{n,i}}$	524.74	$\mathrm{kg \cdot m^2}$
Second moment of area	$I_{\mathrm{t,i}}$	0.15	$\mathrm{m^4}$
Poisson's ratio	ν_{i}	0.3	-
Young's modulus	E_{i}	5.0	GPa
Shear modulus	G_{i}	1.9	GPa
Compressive strength	$\sigma_{\mathrm{c,i}}$	3.0	MPa
Salinity	S_{i}	7.03	‰
Temperature	T_{i}	-10	℃
Brine volume fraction	$\nu_{\mathrm{b,i}}$	38.29	‰
Flexural strength	$\sigma_{\mathrm{f,i}}$	0.56	MPa
Form drag coefficient	$c_{\mathrm{d,f,i}}$	1.0	-
Dynamic viscosity of sea water	μ_{w}	1.88×10^{-3}	Pa·s
Skin friction coefficient[i]	$c_{\mathrm{d,s,i}}$	-	-

Table 4-1 Parameters summary of the level ice model

4.2 Buoy Structure

The buoy structure model is constructed based on the concept design of meso-scale floater by van den Berg et al.[19], a concept map is depicted on Figure 4-1. In this

[i] Depends on the Reynolds number of a specific location.

section, all necessary parameters of the buoy model in a stationary state will be determined in detail.

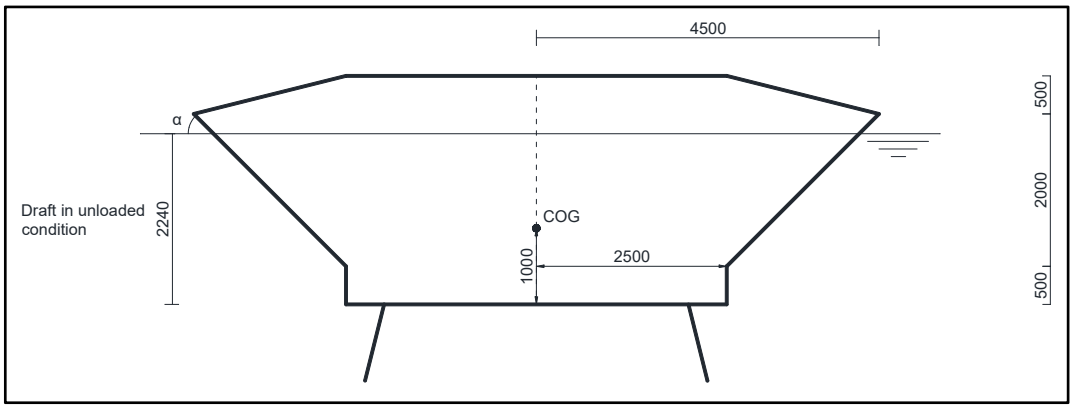

Figure 4-1 A concept buoy design, α=45° (units in mm)

4.2.1 Dimensions

The pre-designed buoy is a hollowed class truncated cone structure. The detailed dimensions in the two-dimensional plane have been depicted in Figure 4-1. To summarize, the following values are the main dimensions (maximum diameter, waterline diameter, minimum diameter (bottom), and height) we use in the buoy model:

$$\begin{aligned} D_{\mathrm{s,max}} &= 9\ \mathrm{m} \\ D_{\mathrm{s,wl}} &= 8.48\ \mathrm{m} \\ D_{\mathrm{s,min}} &= 5\ \mathrm{m} \\ \mathrm{H_s} &= 3\ \mathrm{m} \end{aligned} \tag{4-15}$$

4.2.2 Weight

To obtain the weight, one first needs to calculate the displaced water volume of the buoy, which is determined by dimensions (with stationary draft d_s=2.24 m):

$$V_{\mathrm{d,s}} = \pi\left(\frac{D_{\mathrm{s,min}}}{2}\right)^2 \cdot \frac{H_{\mathrm{s}}}{6} + \frac{\pi}{3}\left(\left(\frac{D_{\mathrm{s,min}}}{2}\right)^2 + \left(\frac{D_{\mathrm{s,wl}}}{2}\right)^2 + \frac{D_{\mathrm{s,min}}}{2}\cdot\frac{D_{\mathrm{s,wl}}}{2}\right)\cdot\left(d_{\mathrm{s}} - \frac{H_{\mathrm{s}}}{6}\right) \tag{4-16}$$

With the displacement, one can calculate the weight using the buoyancy formula:

$$m_{\mathrm{s}} = \rho_{\mathrm{w}} \cdot V_{\mathrm{d,s}} \tag{4-17}$$

4.2.3 Hull Angle

When research into the ice-structure interaction, the most decisive part of the structure is the hull angle. In the case of a buoy performing in the Arctic region, a downward-sloping hull angle can keep the ice bending downwards. The pre-designed buoy model has a downward-sloping hull angle of α and an upward-sloping hull angle of θ, see the summary.

4.2.4 Rotational Properties

In the model, the rotational motion of the structure is around the axis of the ice's width direction. To simulate the rotational motion, the moment of inertia and the second moment of area are needed to be determined first. To avoid complicated calculation, the shape of the hull can be approximated as a hollowed cone with the diameter $D_{s,max}$ here. Thus the moment of inertia is written as (Parallel axis theorem applied here, with the center of gravity 1 m above of the bottom ($\overline{KG} = 1\,\mathrm{m}$)):

$$I_{n,s} = \frac{1}{4} m_s \left(\left(\frac{D_{s,max}}{2} \right)^2 + 2H_s^2 \right) - m_s \cdot \overline{KG}^2 \tag{4-18}$$

To calculate the second moment of area, one needs to determine the thickness of the buoy surface first, which further needs the material density and the surface area.

The material of buoy is assumed as steel, the density is taken as:

$$\rho_s = 7850\ \mathrm{kg/m^3} \tag{4-19}$$

The surface area of the buoy is obtained as below:

$$\begin{aligned} S_s = \pi \Bigg(& 2 \cdot \left(\frac{D_{s,max}}{2} \right)^2 + \sqrt{\left(\left(\frac{D_{s,max}}{2} - \frac{D_{s,min}}{2} \right)^2 + \left(\frac{H_s}{6} \right)^2 \right)} \cdot \left(\frac{D_{s,max}}{2} + \frac{D_{s,min}}{2} \right) \\ & + \sqrt{\left(\left(\frac{D_{s,max}}{2} - \frac{D_{s,min}}{2} \right)^2 + \left(\frac{2 \cdot H_s}{3} \right)^2 \right)} \cdot \left(\frac{D_{s,max}}{2} + \frac{D_{s,min}}{2} \right) + D_{s,min} \cdot \frac{H_s}{6} \Bigg) \end{aligned} \tag{4-20}$$

The equivalent thickness of the buoy hull is thus approximated as:

$$t_s = \frac{m_s}{\rho_s \cdot S_s} \tag{4-21}$$

The second moment of area is used in the calculations regarding the hydrostatic stability, which is obtained as below:

$$\begin{aligned} I_{t,s} = & \frac{D_{s,min} H_s^3}{12} + 2 \left(\frac{1}{36} \left(\frac{5H_s}{6} \right)^3 \cdot \frac{H_s}{6 \cdot \tan\theta} + \frac{1}{2} \cdot \frac{5H_s}{6} \cdot \frac{H_s}{6 \cdot \tan\theta} \left(\frac{H_s}{6} \right)^2 \right) \\ & - \frac{(D_{s,min} - 2t_s)(H_s - 2t_s)^3}{12} \\ & - 2 \left(\frac{1}{36} \left(\frac{5H_s}{6} - 2t_s \right)^3 \left(\frac{H_s}{6 \cdot \tan\theta} - 2t_s \right) + \frac{1}{2} \left(\frac{5H_s}{6} - 2t_s \right) \left(\frac{H_s}{6 \cdot \tan\theta} - 2t_s \right) \left(\frac{H_s}{6} \right)^2 \right) \end{aligned} \tag{4-22}$$

Further, the radius of gyration can be obtained by:

$$R_{g,s} = \sqrt{\frac{I_{n,s}}{m_s}} \tag{4-23}$$

4.2.5 Drag Coefficient

Similar to the level force, the profile drag on the structure also includes the form drag and the skin friction drag.

The form drag coefficient mainly depends on the shape of the structure in the flow. The shape of the buoy under the waterline can be simplified as a circular cylinder. In a Laminar flow, the form drag coefficient for a circular cylinder is given as[20]:

$$c_{\mathrm{d,f,s}} = 1.17 \tag{4-24}$$

The skin friction drag coefficient for the structure, on the other hand, is related to the Reynolds number of the flow. In the Laminar flow, the skin friction drag coefficient is obtained according to Blasius solution:

$$c_{\mathrm{d,s,s}} = \frac{0.664}{\sqrt{\mathrm{Re_s}}} \tag{4-25}$$

where

$$\mathrm{Re_s} = \frac{\rho_{\mathrm{sea}} \dot{u} L_{\mathrm{c,s}}}{\mu_{\mathrm{sea}}} \tag{4-26}$$

which is the Reynolds number, and $L_{\mathrm{c,s}}$ is the characteristic linear dimension of the structure, while μ_{sea} is the dynamic viscosity of the sea water.

4.2.6 Summary

The values of the main parameters about the pre-designed buoy structure at a stationary state are concluded in Table 4-2.

Maximum diameter	$D_{\mathrm{s,max}}$	9	m
Minimum diameter	$D_{\mathrm{s,min}}$	5	m
Waterline diameter	$D_{\mathrm{s,wli}}$	8.48	m
Height	H_{s}	3	m
Draft	d_{s}	2.24	m
Displaced water volume	$V_{\mathrm{d,s}}$	73.28	$\mathrm{m^3}$
Weight	m_{s}	7.51×10^4	kg
Downward-sloping hull angle	α	45	°
Upward-sloping hull angle	θ	14.04	°
Moment of inertia	$I_{\mathrm{n,s}}$	6.43×10^5	$\mathrm{kg\cdot m^2}$
Material density	ρ_{s}	7850	$\mathrm{kg/m^3}$
Surface area	S_{s}	154.66	$\mathrm{m^2}$
Equivalent hull thickness	t_s	0.0619	m
Second moment of area	$I_{\mathrm{t,s}}$	2.05	$\mathrm{m^4}$
Radius of gyration	$R_{\mathrm{g,s}}$	2.93	m
Form drag coefficient	$c_{\mathrm{d,f,s}}$	1.17	-
Skin friction coefficient[ii]	$c_{\mathrm{d,s,s}}$	-	-

Table 4-2 Parameters summary of the buoy structure model

[ii] Depends on the Reynolds number.

4.3 Mooring System

The theory supporting the preliminary design of the mooring lines has been introduced in Section 2.4. In this section, the detailed derivation of the designing process and parameter determinations are carried out.

4.3.1 Equation Derivation

A catenary mooring line configuration is illustrated in Figure 4-2, the angle between the mooring line at the fairlead and the horizontal shown is as angle *j*. The force applied to the mooring line at the fairlead is given as F_m in [N]. The water depth plus the distance between sea level and the fairlead in [m] is d_m in this equation, while w_m is the unit weight of the mooring line in the water in [kg/m].

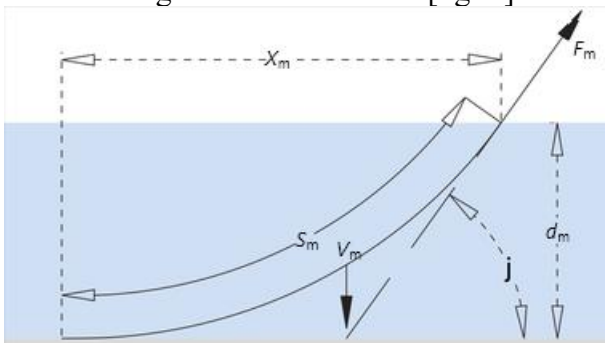

Figure 4-2 Catenary mooring line configuration

A catenary mooring line will have a part which is laying on the seafloor and a part of the mooring line suspended in the seawater. The part that is suspended in the seawater will take on a catenary shape. Depending on the water depth, the weight of the mooring line and the force applied to the mooring line at the fairlead, the length of the suspended mooring line S_m in [m] can be calculated with:

$$S_m = \sqrt{d_m \cdot \left(\frac{2F_m}{w_m g} - d_m \right)} \tag{4-27}$$

The horizontal distance X_m in [m] between the fairlead and the touchdown point of the mooring line on the seabed can be calculated with:

$$X_m = \left(\frac{F_m}{w_m g} - d_m \right) \cdot \ln \left(\frac{S_m + \frac{F_m}{w_m g}}{\frac{F_m}{w_m g} - d_m} \right) \tag{4-28}$$

The weight of the suspended chain *V* in [t] is given by:

$$V_m = w_m \cdot S_m \tag{4-29}$$

The shape of a catenary mooring line is given by the function:

$$y = -\frac{1}{b_m} \cdot \ln\left(\cos\left(b_m \cdot x\right)\right) \tag{4-30}$$

The shape of the catenary line is uniquely ascertained by parameter b_m given by:

$$b_{\mathrm{m}} = \frac{\rho_{\mathrm{m}} \cdot g \cdot A_{\mathrm{m}}}{F_{\mathrm{m,x}}} \tag{4-31}$$

where ρ_{m} is the submerged density of the line material, and A_{m} is the cross section area of the thread, while $F_{\mathrm{m,x}}$ is the normalized horizontal tension component.

Concluded from the derivation above, for a common mooring line, the catenary shape can be determined by four input parameters:
1. The distance between the seabed and the fairlead d_{m}
2. The initial tension of the mooring line at the fairlead F_{m}
3. Normalized thread diameter D_{m}
4. The submerged density of the line material ρ_{m}

4.3.2 Input Parameters

Regarding the catenary mooring system anchoring an offshore buoy, mooring chains are considered the cheapest and most durable solution. Therefore in the current study, the mooring chains are applied in the model as the entity of the mooring lines.

The parameter determinations of the mooring system start mainly from the 4 input values mentioned above. Since mooring chains are employed, the input values are correspondingly adjusted. With the input values determined, the catenary shape of the mooring chains can be determined. The following are the determination of these input values.

Distance between the seabed and the fairlead
The water depth at which the buoy is operating is designed as 30 m. The distance between the seabed and the fairlead can be calculated by subtracting the hull draft from the water depth:

$$d_{\mathrm{m}} = d_{\mathrm{w}} - d_{\mathrm{s}} \tag{4-32}$$

The result is thus:

$$d_{\mathrm{m}} = 27.76\,\mathrm{m} \tag{4-33}$$

Submerged unit weight of the mooring chain
The diameter of mooring lines is primarily determined by the load of its anchoring structure. Since we employ the mooring chain, the relation between the diameter and sectional area is different from that of a common mooring line. In fact, the dimensional relation regarding the mooring chain is complicated. Figure 4-3 shows the dimensions of typical buoy mooring chains according to a handbook (1969) by Myers et al.[21]. The dimensions of a suitable mooring chain can be picked according to the load.

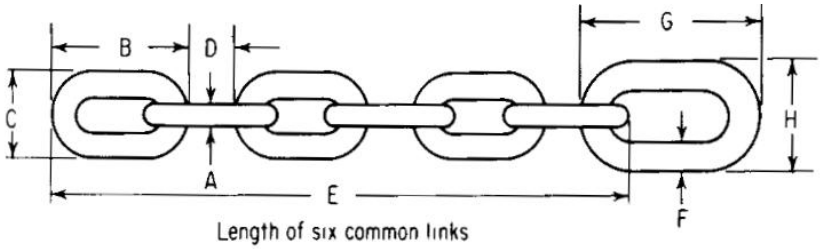

Length of six common links

Common links					End links			Link tolerance, length and width	Proof load, lb	Break load, lb	Wt. per 15 fathoms, lb
Wire diam *A*	Length *B*	Width *C*	Space between ends of links, *D*	Length of six links, *E*	Wire diam *F*	Length *G*	Width *H*				
1/2	3	1 7/8	1	13	3/4	4 1/2	2 5/8	1/32	7,500	15,000	210
5/8	3 3/4	2 1/4	1 1/4	16 1/4	3/4	4 1/2	2 5/8	1/32	11,500	23,000	323
3/4	4 1/2	2 5/8	1 1/2	19 1/2	7/8	5 1/4	3 1/8	1/16	16,000	32,000	442
7/8	5 1/4	3 1/8	1 3/4	22 3/4	1 1/8	6 3/4	3 7/8	1/16	22,000	44,000	608
1	6	3 1/2	2	26	1 1/4	7 1/2	4 3/8	3/32	29,000	58,000	780
1 1/8	6 3/4	3 7/8	2 1/4	29 1/4	1 1/4	7 1/2	4 3/8	3/32	38,500	77,000	990
1 1/4	7 1/2	4 3/8	2 1/2	32 1/2	1 1/2	9	5 1/4	1/8	45,500	91,000	1,245
1 1/2	9	5 1/4	3	39	1 7/8	11 1/4	6 1/2	5/32	65,500	131,000	1,762
1 5/8	9 3/4	5 11/16	3 1/4	42 1/4	1 7/8	11 1/4	6 1/2	5/32	76,500	153,000	2,040
1 3/4	10 1/2	6 1/16	3 1/2	45 1/2	2 1/8	12	7 3/16	3/16	86,500	173,000	2,370
1 7/8	11 1/4	6 1/2	3 3/4	48 3/4	2 1/8	12	7 3/16	3/16	100,000	200,000	2,640

Figure 4-3 Dimensions of buoy chains by Myers et al. (1969)

The selection of the buoy chain dimension is mainly based on its proof load, while the requirement on the horizontal displacement limit of the buoy also influences the selection. In order to minimize the horizontal displacement of the buoy, during the pre-design phase, according to the handbook, the wire diameter (A) can be picked as 1.75 inches (0.0445 m), which corresponds to the weight per 15 fathoms as 2640 lbs. With the units converted, as well as the submerging factor[iii] considered, the submerged unit weight of the mooring chain is obtained as below:

$$w_{\mathrm{m}} = 37.98\ \mathrm{kg/m} \tag{4-34}$$

On the other hand, one of the disadvantages of heavier chains is that the buoy will be pulled downwards due to the weight of the chain. Chains with 1.75-inch wire diameter can pull the buoy down with approximately 6-8 cm, based on their suspended length. Dimensions of the mooring chains can be adjusted afterward according to the practical situation and requirements.

Initial tension of the mooring chain at the fairlead

The initial tension of the mooring chain mainly determines the restoring capability of the mooring system. A higher tension results in a higher restoring coefficient, as well as a higher suspended length, and thus a larger pull-down displacement of the buoy. Figure 4-4 and 4-5 show the initial restoring coefficient and the initial horizontal suspended length as a function of the initial tension, respectively.

[iii] Steel retains about 87% of its mass submerged in seawater.

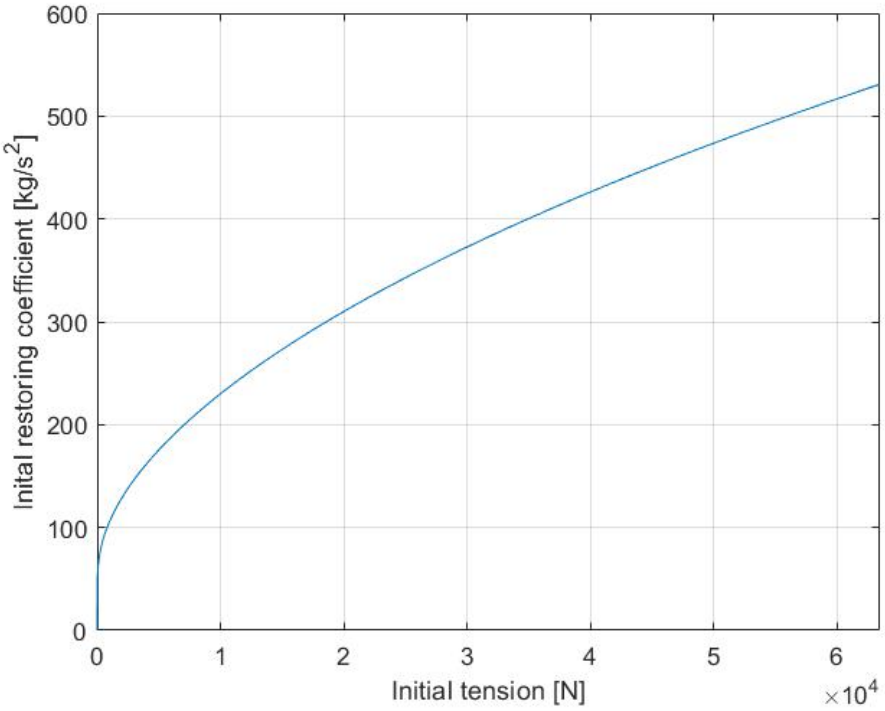

Figure 4-4 Initial restoring coefficient as a function of the initial tension

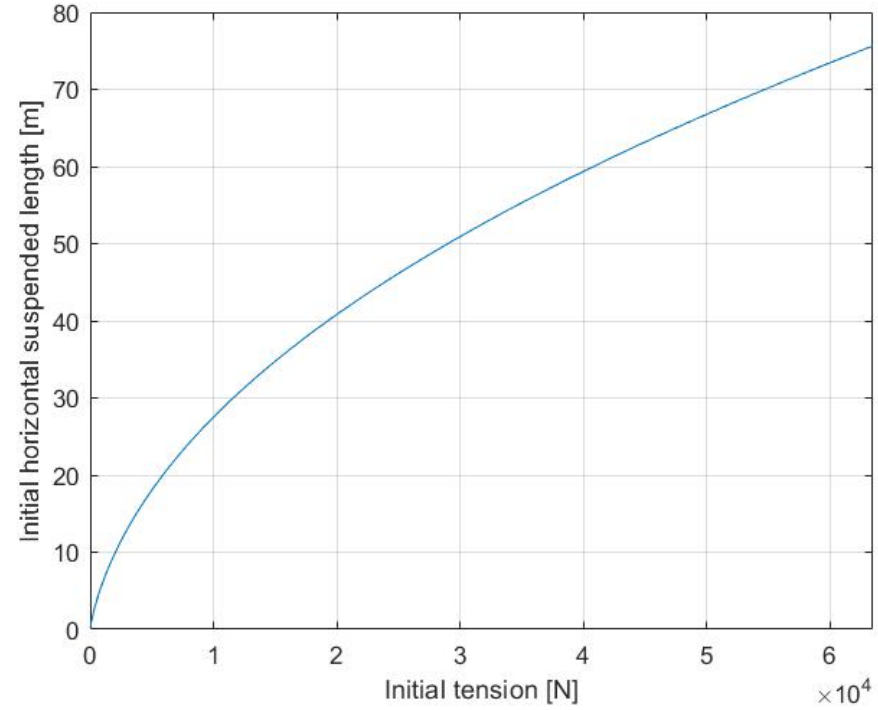

Figure 4-5 Initial horizontal suspended length as a function of the initial tension

To provide the buoy with sufficient restoring capability, and a relatively smaller pull-down displacement, the initial horizontal suspended length can be chosen as 45 m. The corresponding mooring tension at fairlead is thus:

$$F_{\mathrm{m}} = 2.54\times10^{4}\ \mathrm{N} \tag{4-35}$$

Distance between the anchor and the initial touchdown point & Total chain length

With the horizontal displacement of the buoy, the touchdown point moves as well. To avoid that the touchdown point coincides with the anchor point (the mooring chain fully suspended), the distance between the anchor and the initial touchdown point should be sufficiently large, which also indicates that the total chain length should be sufficiently long. The relation of these two parameters are shown below:

$$L_{\mathrm{m}} = D_{\mathrm{m,a}} + S_{\mathrm{m}} \tag{4-36}$$

where L_{m} is the total length of the mooring chain, while $D_{\mathrm{m,a}}$ is the distance between the anchor and the initial touchdown point.

The determination of these two parameters is mainly related to the horizontal displacement limit of the buoy. For a small-scale structure like the buoy, a scope[iv] of 5:1 is recommended[22]. Therefore, the total length is 138.80 m, and thus the distance between the anchor and the initial touchdown point is 83.90 m. These two parameters can also be adjusted afterward according to the practical situation and economic requirement.

4.3.3 Summary

The values of the main parameters of a pre-designed mooring chain at a stationary state are concluded in Table 4-3.

Distance between the seabed and fairlead	d_{m}	27.76	m
Initial tension of the mooring chain at the fairlead	F_{m}	2.54×10^{4}	N
Wire diameter (A)	-	0.0445	m
Submerged unit weight of the mooring chain	w_{m}	37.98	kg/m
Initial horizontal suspended length	X_{m}	45	m
Weight of the suspended chain	V_{m}	2.09×10^{3}	kg
Length of the suspended mooring chain	S_{m}	54.90	m
Distance between the anchor and the initial touchdown point	$D_{\mathrm{m,a}}$	83.90	m
Total chain length	L_{m}	138.80	m
Catenary shape parameter	b_{m}	0.0231	-
Distance between a fairlead and its nearby bottom edge	$d_{\mathrm{m,f}}$	0.5	m

Table 4-3 Parameters summary of the mooring system

4.4 Conclusion

This chapter gives comprehensive parameter determinations for the whole model. The parameters determined in this Chapter provides the numerical model with most of the input values. At the same time, the parametric study also further illustrates the idea of model construction.

[iv] Total chain length / Distance between the seabed and fairlead

On the other hand, it must be pointed out that some parameters are determined as not sufficiently optimized due to the limit of the simulating duration. Besides, some parameters are not fixed as well, for instance, the parameters for the mooring system are determined preliminarily, which can be further modified for a more optimized result.

Further, the result and its verification of the simulation are shown in Chapter 5, and the optimization will be carried out in Chapter 6.

5

MODEL VERIFICATION

So far, the construction of the numerical model has been mostly completed, and the input values have been preliminarily determined as well. In this chapter, the results from the current model simulation will be demonstrated, while the verification for the model will be performed based on the results, to ensure the numerical model is correctly constructed.

The method of verification in the current study generally includes the analytical solution and the ordinary differential equation - medium order method (ode45 solver), which can both be performed by MATLAB. In the meantime, some results will be verified by comparing with previous simulation results.

Besides, it should be noted that only the mechanism of implicit forces, which involves the Lagrange multiplier formulation, is necessary to be verified; while since the explicit force is processed by applying the acceleration vector in the time-loop control, it is, in fact, solved analytically, and thus not necessary to be verified additionally.

5.1 Level Ice Model

The aim for this verification is to ensure the steady state of the level ice model under a certain load is sufficiently accurate. In this way, any damping coefficients can be neglected. Therefore, an analytical solution of the steady state is applied as a method of verification.

The following verification is based on a level ice model floating on the sea water. The level ice has both sides free, and no interaction with structure, but instead with a point load on one of the free side.

5.1.1 Analytical Solution

The level ice model is verified by the analytical solution. The following are the detailed derivation of the analytical solution.

We assume a semi-infinite beam, subjected to a point load on a free edge. The derivation of the analytical solution is implemented as below:

The governing equation of a semi-infinite beam on an elastic foundation is formed as:

$$EI\frac{d^4w}{dx^4}+kw=0 \tag{5-1}$$

The general solution of a semi-infinite beam on an elastic foundation is sought as:

$$w(x) = e^{-\beta x}\left(C\cos\beta x + D\sin\beta x\right) \tag{5-2}$$

where

$$\beta = \left(\frac{k}{4EI}\right)^{\frac{1}{4}} \tag{5-3}$$

while C and D are integration constants. Then the bending moment and shear force are:

$$M = EI\frac{\mathrm{d}^2 w}{\mathrm{d}x^2}, \quad T = EI\frac{\mathrm{d}^3 w}{\mathrm{d}x^3} \tag{5-4}$$

At x=0, the beam is subjected to a concentrated load P. The constants C and D can be ascertained by applying the following boundary conditions at the left end of the beam:

$$M\left(x=0\right)=0, \quad T\left(x=0\right)=P \tag{5-5}$$

The results are

$$C = \frac{P}{2\beta^3 EI} = \frac{2P\beta}{k}, \quad D = 0 \tag{5-6}$$

The deflection is now found by substituting C and D into the general solution (5-2) as

$$w(x) = \frac{Pe^{-\beta x}}{2\beta^3 EI}\left(\cos\beta x\right) \tag{5-7}$$

The bending moment and shear force can also be calculated:

$$\begin{aligned} M\left(x\right) &= \frac{Pe^{-\beta x}}{\beta}\left(\sin\beta x\right) \\ T\left(x\right) &= -Pe^{-\beta x}\left(\sin\beta x - \cos\beta x\right) \end{aligned} \tag{5-8}$$

Substituting known values into the formula (5-8), one can plot a figure of the beam shape.

5.1.2 Result Verification

For verification, corresponding results of the numerical simulation for the level ice model subjected to a point load are presented. To verify thoroughly, 4 different input conditions varying from total lengths and numbers of elements are tested. The following figures are comparisons about the ice beam deformation between the analytical solution and the numerical simulation.

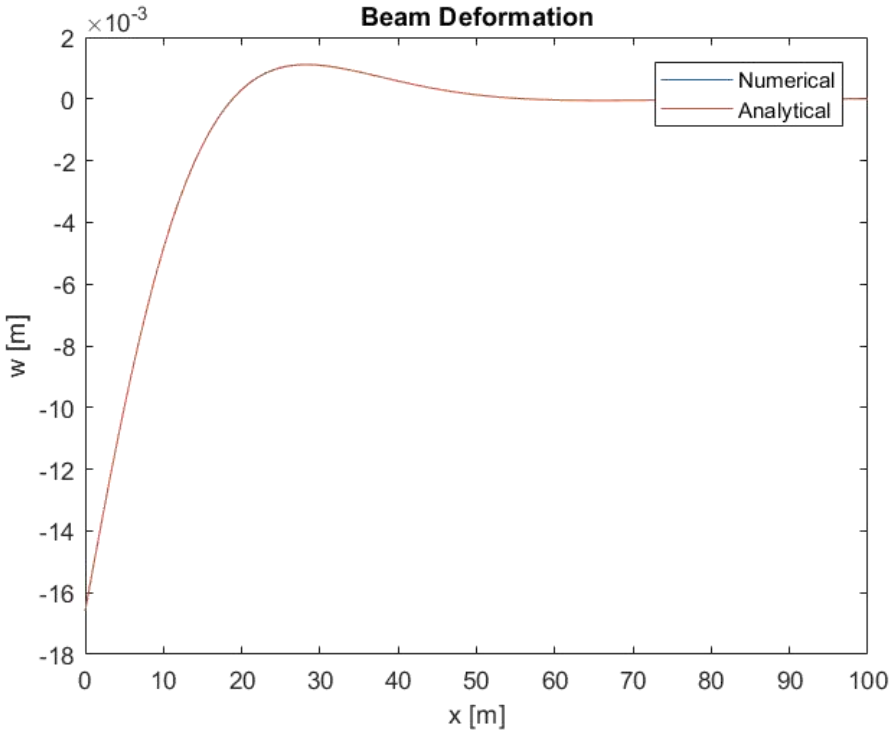

Figure 5-1 Beam deformation verification (n = 100, L = 100 m)

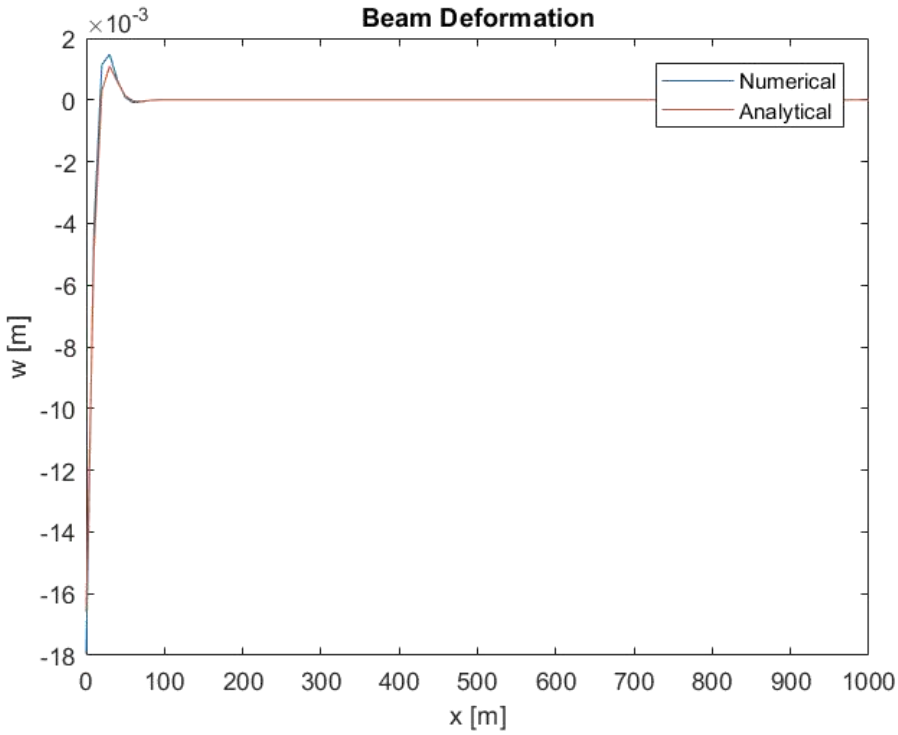

Figure 5-2 Beam deformation verification (n = 100, L = 1000 m)

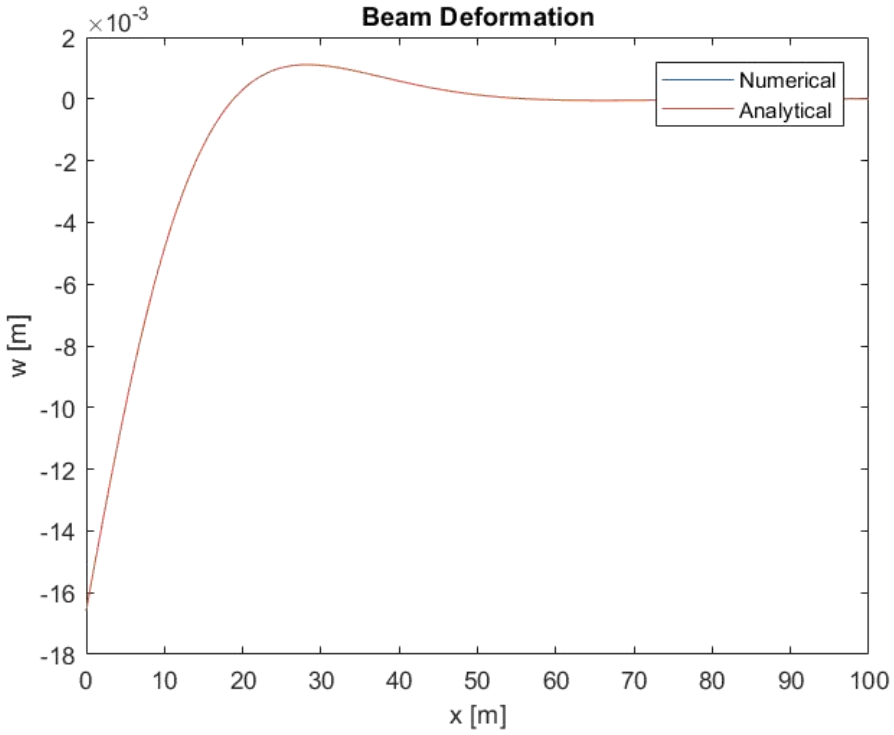

Figure 5-3 Beam deformation verification (n = 1000, L = 100 m)

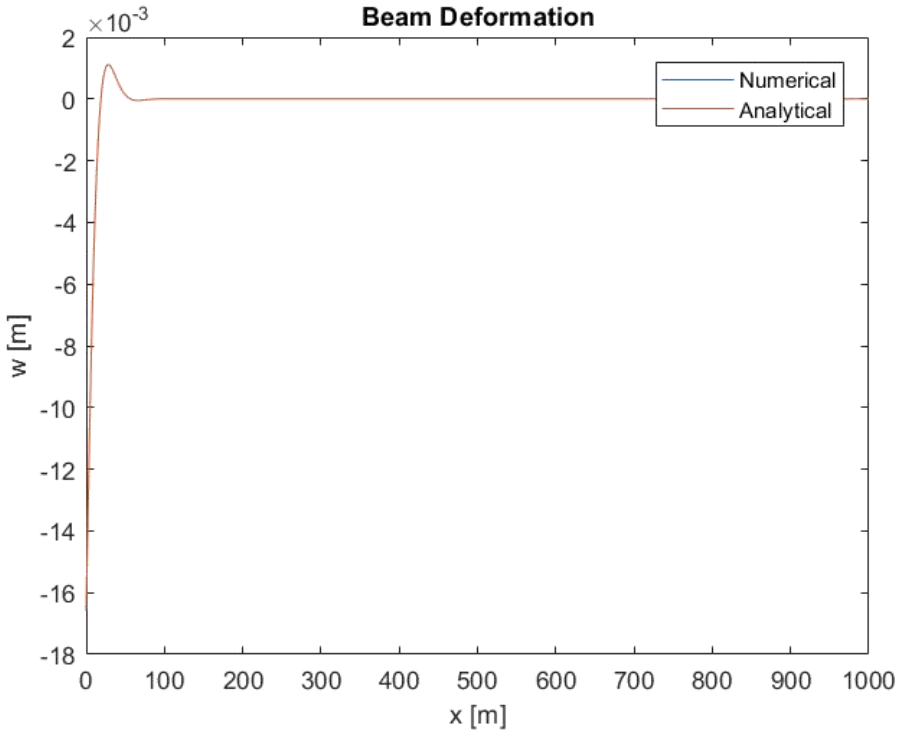

Figure 5-4 Beam deformation verification (n = 1000, L = 1000 m)

As is shown in the figures, the number of elements influences the accuracy of the simulation results. The larger the number of elements is, the closer the simulation results to the analytical solution.

The result of the verification shows tiny errors, within the scope of 10^{-5} m. Therefore, it can be confirmed that the result of numerical simulation for the beam deformation is correct.

For the bending moment and the shear force, we take the case of [L=100 m, n=100] for verification. The following figures are the results of the verification for the bending moment and the shear force:

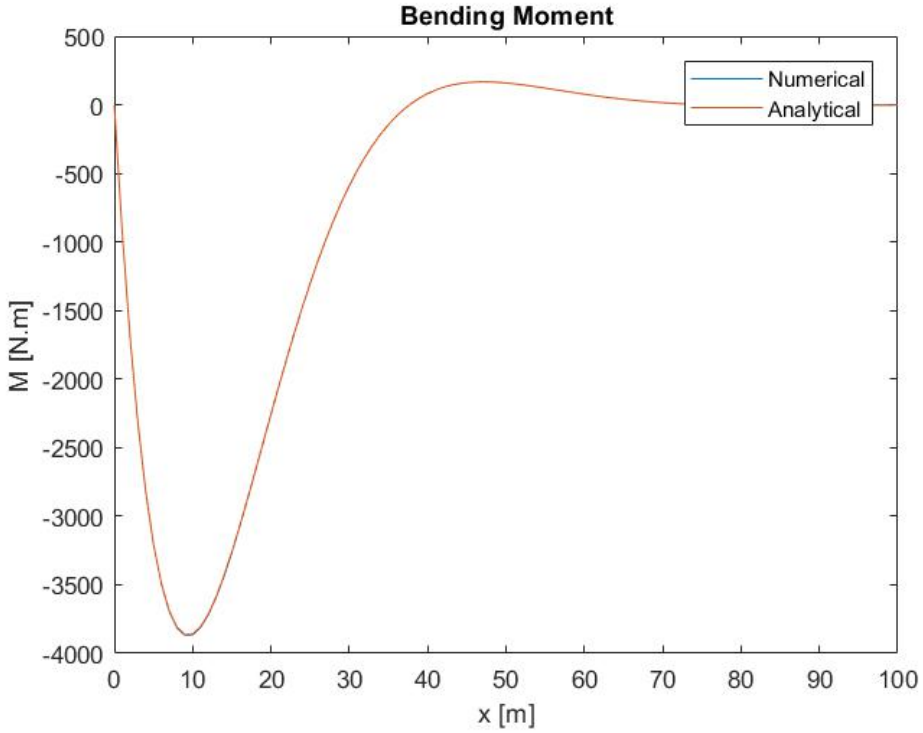

Figure 5-5 Bending moment verification (n=100, L=100 m)

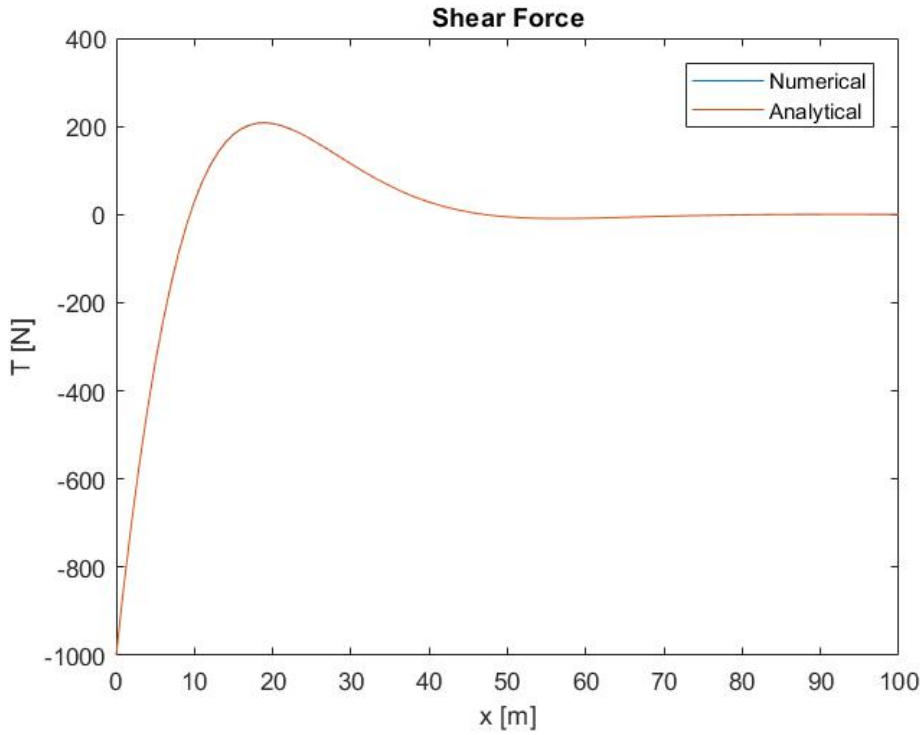

Figure 5-6 Shear force verification (n=100, L=100 m)

The figures above show that the two curves almost completely overlap with each other, which indicates only tiny errors exist between two methods. Therefore, it can be confirmed that the results of the numerical simulation for the beam bending moment and shear force are correct.

With all the above verification correct, one can confirm that the level ice model has been constructed correctly.

5.2 Moored Structure Model

In general, the mechanism of the moored structure model includes the righting moments induced by both the structure's buoyancy and the mooring system, and the restoring force induced by the mooring system.

The only implicit force mechanism applied in the model above is the restoring force. Therefore, the verification of the moored structure model only focuses on the performance of the mooring system.

5.2.1 Ordinary Differential Equation - Medium Order Method (ode45)

Since the restoring force is divided into two components: the linear component and the non-linear component, we want to investigate the behavior of the moored structure in time during the simulation, to confirm that the treatment of linear and nonlinear components is sufficiently accurate. The ode45 solver in MATLAB is capable of calculating the displacement, velocity of an element at any time point with a precision of medium order. Therefore, in the current study, we choose the ode45 solver as a method of verification.

Different from the Lagrange multiplier formulation, the ode45 solver doesn't split the restoring force into two components, but rather treat the whole restoring force as one external force. Noted that any other external forces are neglected here.

The governing equation for the ode45 solver is written as:

$$\dot{q}_n = \begin{bmatrix} \dot{x}_n \\ \ddot{x}_n \end{bmatrix} = \begin{bmatrix} \dot{x}_n \\ -\dfrac{F_{\mathrm{R}}}{m_{\mathrm{s}}} \end{bmatrix} \tag{5-9}$$

where m_{s} is the weight of the structure, and F_{R} is the restoring force.

5.2.2 Result Verification

The input values are identical with those parameters determined in Chapter 4, except for the weight. We choose a smaller value of the weight, to observe the full trail of oscillation in a shorter duration. The result of displacement verification is shown in Figure 5-7.

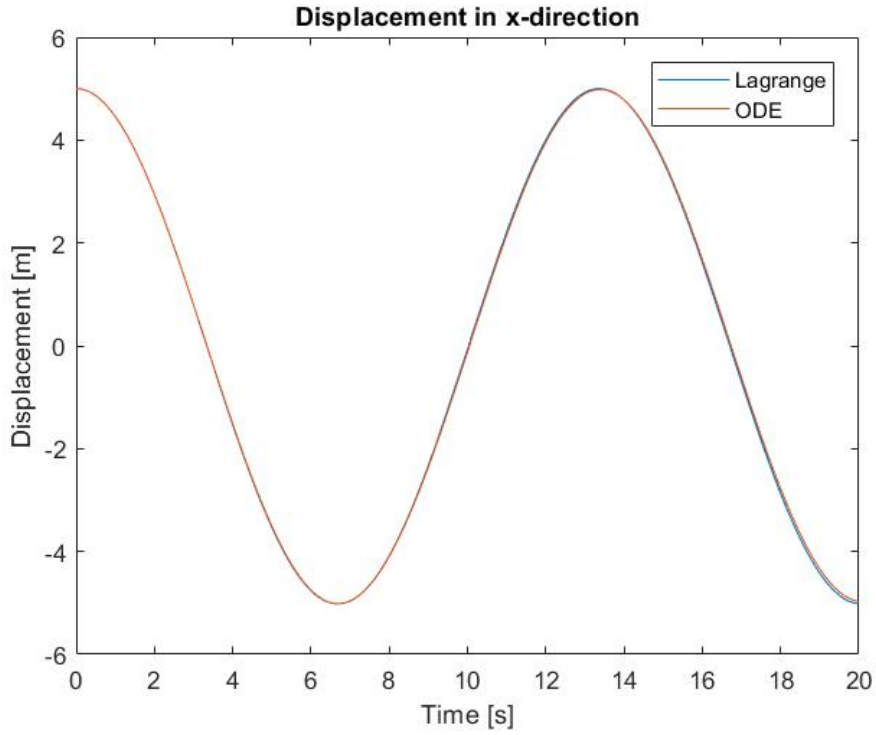

Figure 5-7 Displacement verification of the moored structure

The figure above shows that the two curves almost completely overlap with each other, which indicates only tiny errors exist between two methods. Therefore, it can be confirmed that the restoring force is modeled correctly using the Lagrange multiplier formulation.

5.3 Ice-Structure Contact

With the numerical simulation, we can obtain a series of outputs as a function of time. The verification can be performed in two parts: to verify the model construction mechanisms, namely the conditions listed in Section 3.4.1; to verify by performing the analytical solution.

5.3.1 Verification of Contact Mechanisms

The initial profile of the verifying model is shown in Figure 5-8.

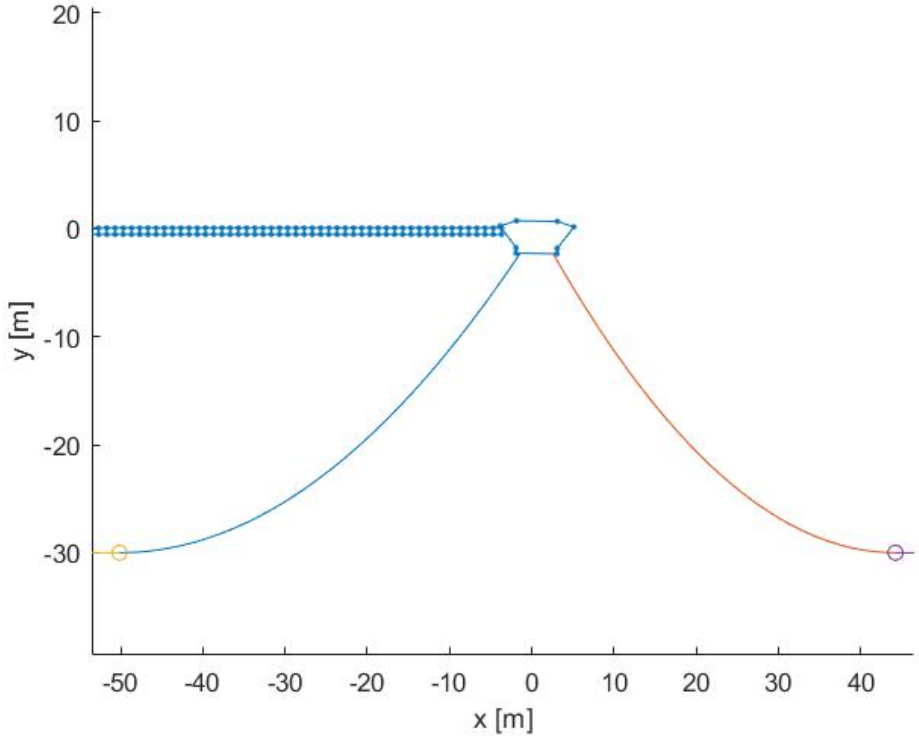

Figure 5-8 Initial profile of the ice-structure contact verification model

Initial conditions and necessary inputs regarding the model are listed in Table 5-1.

Initial horizontal displacement of the structure[i]	0	m
Initial horizontal velocity of the structure	0	m/s
Initial horizontal displacement of the level ice[ii]	-0.1	m
Initial horizontal velocity of the level ice	0.1	m/s
Time-step length	0.001	s
Simulation duration	8	s

Table 5-1 Inputs for the ice-structure contact verification

The results of the simulation can be observed from the following aspects as a function of time, which will prove the conditions are satisfied:

Normal contact force

The resulting figure of the (average) normal force at the contact area is shown below.

[i] Zero value indicates the center of gravity of the structure is at $x = 0$.

[ii] Zero value indicates given that the center of gravity of the structure is at $x = 0$, the relative displacement between two contact points is 0.

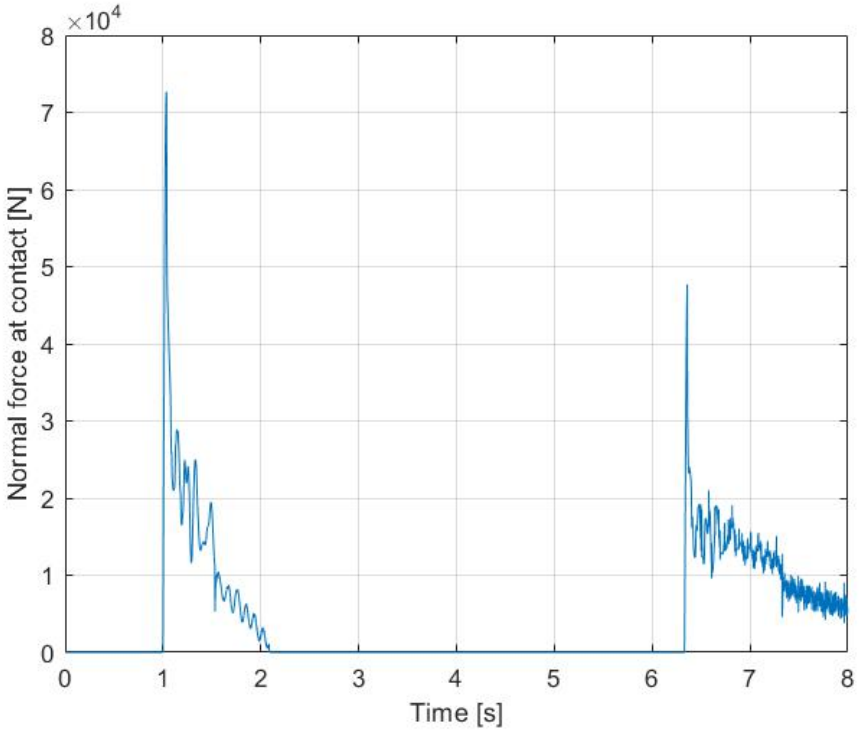

Figure 5-9 Simulation result for the normal force at the contact area

As it is shown in Figure 5-9, in the first time step of the contact, there is a single peak on the curve, the reason of this peak is the impact effect due to the significant change of relative velocity at the moment of the first contact. Then the figure shows a series of oscillation with a decreasing tendency, as the result of relative sliding of the contact surface and consequently the contact points changing over time. From the figure, one can observe that the buoy is being pushed away by the ice during the first contact phase (from $t \approx 1$ s to $t \approx 2.1$ s), and the ice contacts with the buoy again at $t \approx 6.3$ s. From $t \approx 2.1$ s to $t \approx 6.3$ s, the contact force remains as zero, which indicates that the system is under the no-contact phase. In addition, the figure concludes that at the beginning of any time-step, the normal contact force is higher than or equal to zero. Therefore, the condition (2) is met.

Relative displacement (Penetration)

Figure 5-9 can be further compared with the penetration figure to check if the condition (3) is met.

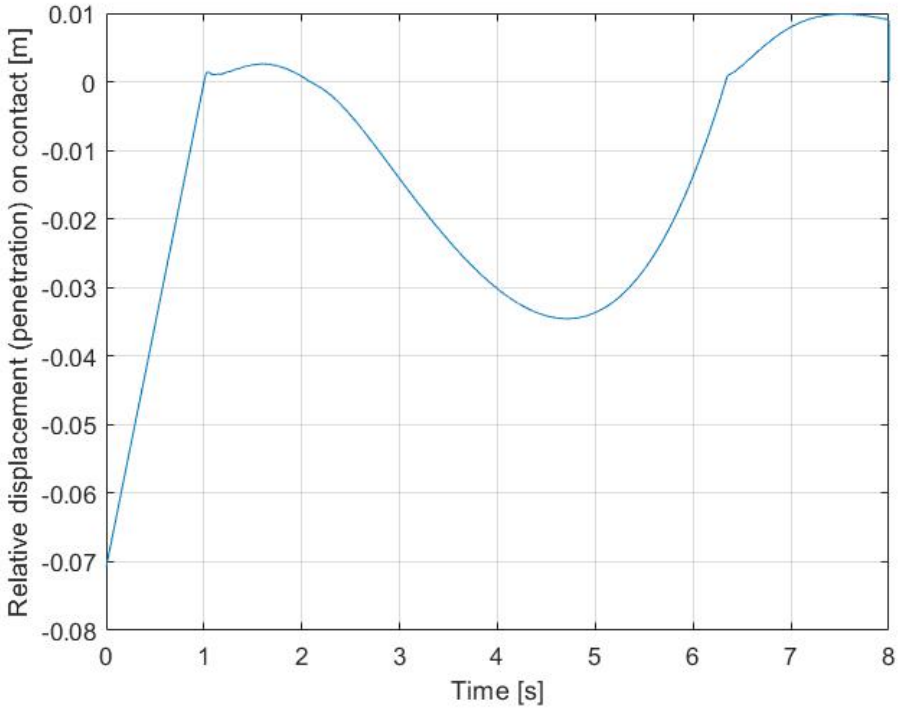

Figure 5-10 Simulation result for the relative displacement (penetration) of contact points

Figure 5-10 shows the positive range of the penetration coincides with the positive range of the contact force in Figure 5-8, which concludes that the contact force exists only when the penetration is larger than or equal to zero. Therefore, one can confirm that the condition (3) is satisfied.

Contact impulse

The values of the contact impulse are limited by the Gauss-Seidel method, the resulting figure is shown as below.

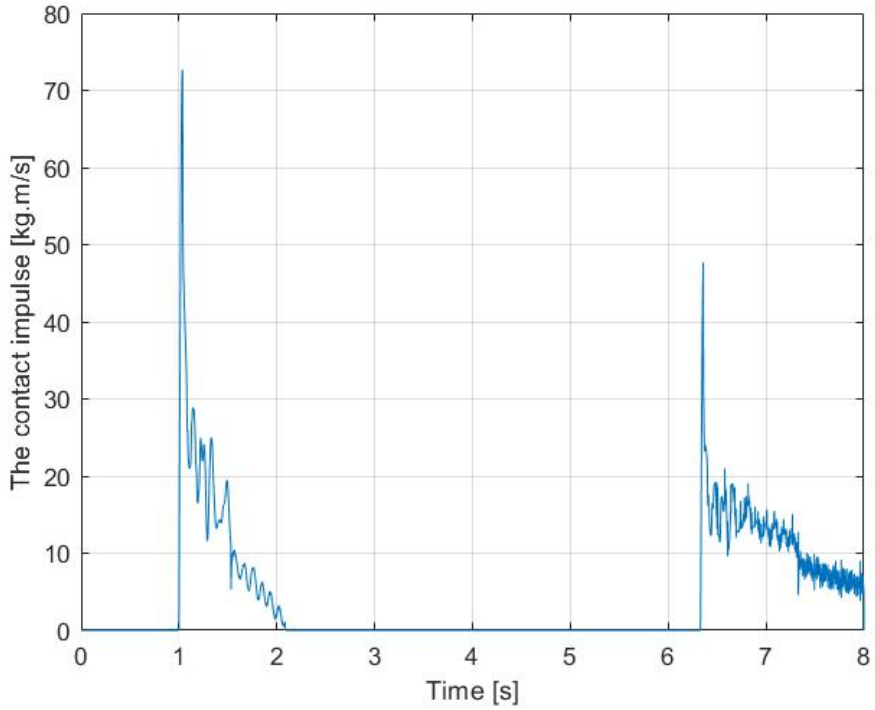

Figure 5-11 Simulation result for the contact impulse

As it is shown in Figure 5-11, the contact impulse retains non-negative during the whole time. Therefore, the condition (4) is proved to be satisfied.

Relative velocity

The condition (5) is verified by contact impulse with the contact force needed to make the relative velocity zero. This condition will keep the relative velocity positive and stable during the contact phase. Figure 5-12 shows the result of the relative velocity.

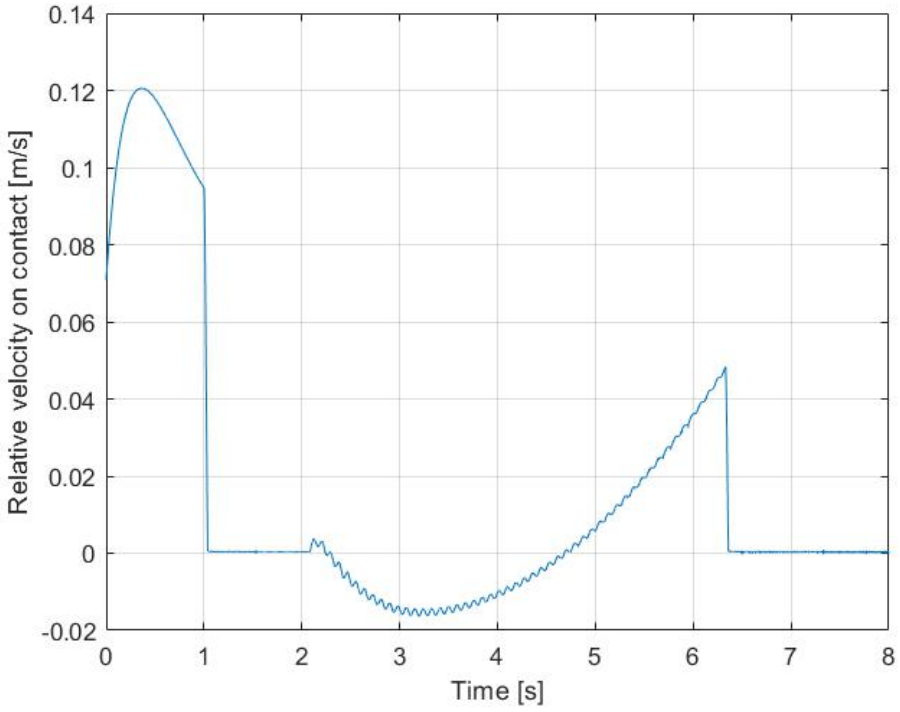

Figure 5-12 Simulation result for the relative velocity of contact points

The condition (5) is satisfied by applying the Gauss-Seidel method. From Figure 5-12, one can conclude that during the contact phase, the relative velocity is positive and relatively stable.

5.3.2 Verification by the Analytical Solution

The verification of the ice-structure contact can be performed by applying an analytical solution for the normal force at the first time-step of the contact phase.

Since the average normal force at the contact point during the contact phase has been numerically simulated, it is necessary to check its correctness by performing the analytical solution. However, due to the condition (5) mentioned in Section 3.4.1, the impulse during the contact phase is changed due to the maximum impulse limit. Therefore, we can only perform the analytical check for the first force peak. The analytical solution for the average normal force is given as:

$$F_{\mathrm{c}} = -k_{\mathrm{c}} \cdot u_{\mathrm{r}} - \frac{2\dot{u}_{\mathrm{r,av}}}{CF_{\mathrm{c}} \cdot \Delta t} \tag{5-10}$$

where u_{r} is the relative displacement (penetration) at the contact point, and $\dot{u}_{\mathrm{r,av}}$ is the average relative velocity at the contact point within two time-steps, while CF_{c} is the compliance factor of the contact.

The derivation is illustrated as below:

$$\begin{aligned} F_{\mathrm{n,av}} &= -\frac{u_{\mathrm{r}}k_{\mathrm{c}} + \dot{u}_{\mathrm{r}}c_{\mathrm{c}} + \left(u_{\mathrm{r}} + \dot{u}_{\mathrm{r}}\Delta t + \frac{1}{2}\Delta\dot{u}_{\mathrm{r}}\Delta t\right)k_{\mathrm{c}} + \left(\dot{u}_{\mathrm{r}} + \Delta\dot{u}_{\mathrm{r}}\right)c_{\mathrm{c}}}{2} \\ &= -\left(k_{\mathrm{c}}u_{\mathrm{r}} + \frac{1}{2}k_{\mathrm{c}}\dot{u}_{\mathrm{r}}\Delta t + \frac{1}{4}k_{\mathrm{c}}\Delta\dot{u}_{\mathrm{r}}\Delta t + c_{\mathrm{c}}\dot{u}_{\mathrm{r}} + \frac{1}{2}c_{\mathrm{c}}\Delta\dot{u}_{\mathrm{r}}\right) \\ &= -k_{\mathrm{c}}u_{\mathrm{r}} - \left(2\dot{u}_{\mathrm{r}} + \Delta\dot{u}_{\mathrm{r}}\right)\left(\frac{1}{4}k_{\mathrm{c}}\Delta t + \frac{1}{2}c_{\mathrm{c}}\right) \end{aligned} \tag{5-11}$$

Since

$$\begin{aligned} CF_{\mathrm{c}} &= \frac{1}{\frac{1}{4}k_{\mathrm{c}}\Delta t^2 + \frac{1}{2}c_{\mathrm{c}}\Delta t} \\ \dot{u}_{\mathrm{r,av}} &= \frac{1}{2}\left(2\dot{u}_{\mathrm{r}} + \Delta\dot{u}_{\mathrm{r}}\right) \end{aligned} \tag{5-12}$$

Substitution gives:

$$F_{\mathrm{c}} = -k_{\mathrm{c}} \cdot u_{\mathrm{r}} - \frac{2\dot{u}_{\mathrm{r,av}}}{CF_{\mathrm{c}} \cdot \Delta t} \tag{5-13}$$

with the contact stiffness k_{c} and the contact damping c_{c}.

The relative displacements and relative velocities of contact points before and after the first time-step from the numerical simulation are read as:

$$\begin{aligned} d_{\mathrm{r}}^{-} &= -3.78\times10^{-7}\ \mathrm{m}, \quad d_{\mathrm{r}}^{+} = 7.03\times10^{-5}\ \mathrm{m} \\ v_{\mathrm{r}}^{-} &= 0.0946\ \mathrm{m/s}, \quad v_{\mathrm{r}}^{+} = 0.0941\ \mathrm{m/s} \end{aligned} \tag{5-14}$$

From the numerical result, the value of the normal contact force at the first time-step of the first and the second contact phases are read respectively as:

$$F_{\mathrm{c},1} = 2.3768\times10^{3}\ \mathrm{N} \quad F_{\mathrm{c},2} = 1.6910\times10^{3}\ \mathrm{N} \tag{5-15}$$

And the results from the analytical solution gives:

$$F_{\mathrm{c},1} = 2.3818\times10^{3}\ \mathrm{N} \quad F_{\mathrm{c},2} = 1.6962\times10^{3}\ \mathrm{N} \tag{5-16}$$

There are only minor errors in the two sets of results. Considered the complexity of the impact effect, the errors are acceptable. Therefore, we can confirm that the result of the numerical simulation of the normal force is sufficiently accurate.

5.4 Ice Bending Failure

The verification on the mechanism of the ice bending failure mainly focuses on the breaking length.

5.4.1 Verifying Model

To achieve the verification, a verifying model is employed, which is depicted in Figure 5-13. The level ice, located at $x \leq 0$, has parameters identical to that determined in Table 4-1. It is assumed that the level ice moves with a constant horizontal velocity v_{ice} towards a structure. The structure is assumed rigid and immovable, and its geometry is ignored except for the hull angle α.

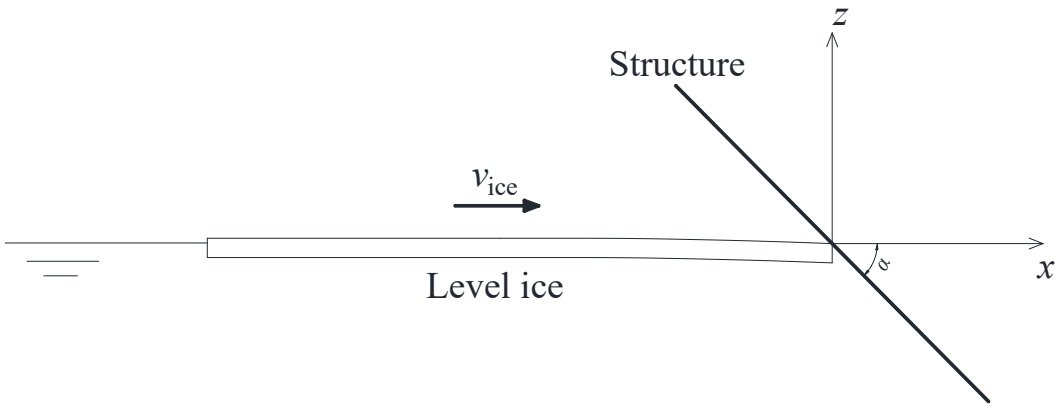

Figure 5-13 Verifying model of the ice breaking length

To perform the verification, a series of horizontal velocities v_{ice} is applied. When the level ice breaks due to bending failure for the first time during the simulation, the

simulation is stopped. Besides, in the other case, if the level ice never breaks due to weak impact in a low velocity, the breaking length will not be recorded. After the whole series of simulations, the observed breaking lengths are recorded. To compare the results with results from a similar numerical simulation performed by C. Keijdener et al.[23], input values of ice properties are kept consistent, see Table 5-2.

Minimum velocity	0.01	m/s
Velocity step between each simulation	0.01	m/s
Maximum velocity	0.5	m/s
Time-step length	0.005	s
Structure's hull angle	45	°
Thickness	1	m
Density	925	kg/m^3
Young's modulus	5×10^9	Pa
Poisson's ratio	0.3	-
Compressive strength	6×10^5	Pa
Flexural strength	5×10^5	Pa
Total length	500	m
Number of element	1000	-
Element length	0.5	m

Table 5-2 Inputs for the ice bending failure verification

5.4.2 Static Breaking Length

To study the features of breaking length, we need first to obtain the static breaking length, which is the length where the highest flexural stress occurred in a static state. The level ice model reaches the static state whenever the failure limit is not reached by the ice's flexural stress. The length where the highest flexural stress occurred in a static state is thus observed:

$$x_{\mathrm{bl}} = 16.5\ \mathrm{m} \tag{5-17}$$

The result of the static breaking length can be verified by the analytical solution derived by Keijdener:

$$x_{\mathrm{bl}} = \sqrt{2}l \arctan\left(\frac{\sqrt{2}l}{\sqrt{2}l - t_{\mathrm{i}}\tan\alpha}\right) \tag{5-18}$$

where

$$l = \sqrt[4]{\delta} \tag{5-19}$$

where

$$\delta = \frac{E_{\mathrm{i}} t_{\mathrm{i}}^3}{\left(12\rho_{\mathrm{w}} g\right)\left(1-\nu_{\mathrm{i}}^2\right)} \tag{5-20}$$

The result is thus:

$$x_{\mathrm{bl}} = 16.74\ \mathrm{m} \tag{5-21}$$

The result from the simulation is 16.5 m, which is close to the analytical solution. Therefore, we can confirm the static breaking length simulated is correct. Noted that the ice element length used in the simulation is 0.5 m, which means the minimum

variation of the breaking length is 0.5 m. Decreasing the value of ice element length will produce a more accurate result in the simulation.

5.4.3 Breaking Length as a Function of Ice Velocity

Figures 5-14 show the results of breaking length as a function of ice velocity.

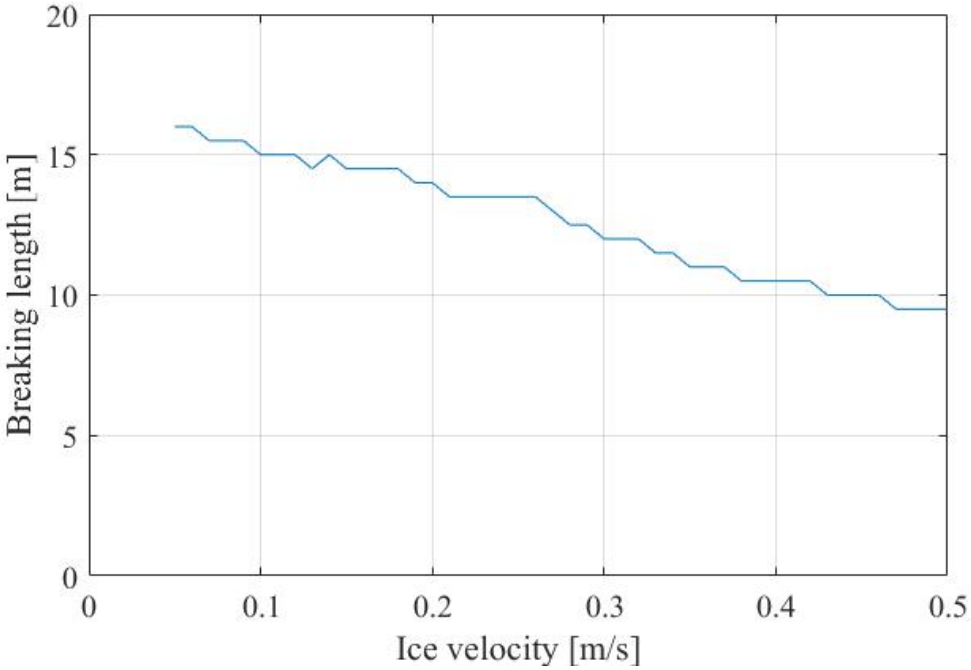

Figure 5-14 The breaking length as a function of ice velocity[iii]

The result above can be compared with the simulation result by C. Keijdener, see the dotted curve shown in Figure 5-15.

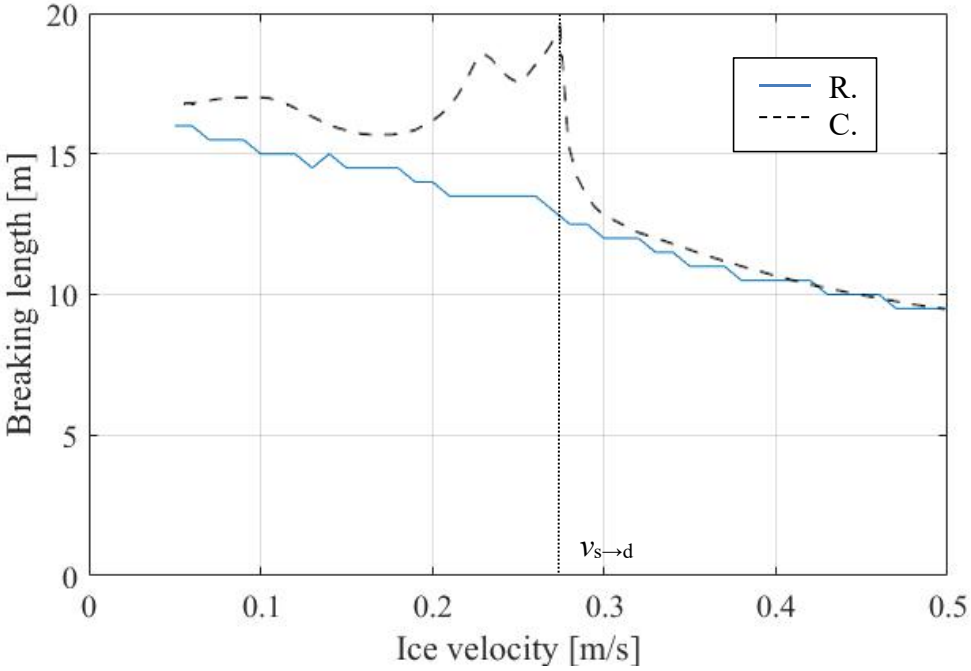

Figure 5-15 The breaking length as a function of ice velocity compared with the result by C. Keijdener

[iii] Increasing the number of ice elements (decreasing the value of ice element length) will produce a smoother and more accurate curve, however, it costs more time to perform the simulation.

According to Keijdener, in the regime of the quasi-static failure mode ($v < v_{s\to d}$), the ice will fail with a breaking length approximately equal to the static breaking length. While in the regime of the dynamic failure mode ($v > v_{s\to d}$), the magnitude of the peak contact force continues to grow as v_{ice} increases, which causes the ice to fail earlier and closer to the contact point.

In Keijdener's curve (C.), the breaking length reaches a peak when the velocity reaches the transition velocity $v_{s\to d}$, while my curve (R.) shows a relative monotonically decreasing tendency. This difference is mainly due to the different damping values applied, where higher damping values are applied in my model. Both curves start approximately from the static breaking length and come to an approximate coincide after the transition velocity.

The simulation result confirms the statement above, together with the verification in Section 5.4.2, the results indicate that the mechanism of the ice bending failure in the model is correctly constructed.

5.5 Conclusion

The verification has been performed in order to gain the confidence of correctness in the constructed numerical model. In summary, there are generally four core aspects in the numerical model verified:

1. The level ice model is verified in aspects of the deformation, the shear force, and the bending moment, given the condition that it is subjected to a point load on one of the free edge. The results are compared with the analytical solution, which gives a positive verification.
2. The moored structure model is mainly verified in the aspect of its mooring restoring force. The simulation result is verified by the ode45 method, while the result shows the sufficient correctness.
3. The ice-structure contact is verified by examining if the simulation results satisfy 5 conditions of the contact mechanism. Besides, the normal force at the first time-step of the contact phase is verified by the analytical solution. The results of the verification sufficiently show the correctness of the contact mechanism in the numerical model.
4. The ice bending failure is verified in two aspects: the static breaking length and the breaking length as a function of ice velocity. The former is verified by the analytical solution, while the latter is verified by comparing the result with the corresponding result obtained by Keijdener et al. Both processes of the verification have indicated the correctness of the bending failure mechanism.

6

BUOY DESIGN OPTIMIZATION

Now that the numerical model has been constructed and verified, it is possible to optimize the buoy design for a specific ice condition. In this chapter, an example of the optimization of the moored buoy model is demonstrated.

6.1 Optimization Overview

The optimization will focus on the moored buoy in the current Arctic region, based on the pre-designed buoy presented in Section 4.2. The basic idea of the optimization plan is:
'To obtain a concept design of a satisfactorily performed moored buoy with minimized dimensions under a specific ice condition'

The above 'a specific ice condition' refers to the level ice determined in Section 4.1. The level ice has a constant velocity of 0.1 m/s towards the buoy in a normal condition, and that of 0.2 m/s in an extreme condition.

To achieve the objective of the optimization, the buoy design is needed to satisfy the following criteria:

(1) The buoy is not allowed to overturn into water under both ice conditions;
(2) The buoy has a constant hull thickness and total height, see Table 4-2;
(3) The stationary draft has a range of [0.5,2.5] m to make sure the level ice contacts with the downward-sloping hull (taking 5% as the safety factor, the range is limited to [0.6,2.4] m);
(4) The upward-sloping hull of the buoy is not allowed to be submerged into water under the normal ice condition;
(5) The maximum horizontal displacement of the buoy is not allowed to exceed 15% of water depth under the normal ice condition;
(6) The maximum pitch angle is not allowed to exceed 15° under the extreme ice condition;
(7) The maximum horizontal displacement of the buoy is not allowed to exceed 25% of water depth under the extreme ice condition.

With the above criteria, the buoy design with minimized total weight (including the weight of the buoy and the mooring chain) is the most optimized design.

Under this circumstance, the following are the main variables for the optimization of the buoy design to investigate:

1. The downward-sloping hull angle of the buoy;
2. The maximum diameter of the buoy;

Generally, size parameters like the maximum diameter influence the buoy's hydrostatic stability. With the change of the hull angle, the minimum diameter also changes. Overall, the size parameters determine the buoy's weight given that the hull thickness is constant. Moreover, the hull angle influences the interaction between the level ice and the buoy, which indirectly affects the stability of the buoy.

The optimization is performed with a series of numerical simulations, based on the results including the maximum pitch angle and maximum horizontal displacement of the buoy, the best solution is chosen and further adjusted.

6.2 Optimization Process

To investigate the optimization, preliminary setting ranges for the two size-related variables are listed in Table 6-1, which are based on the pre-designed dimensions in Table 4-2.

Item	Minimum	Variation	Maximum	Unit
Maximum diameter	7	0.5	10.5	m
Hull angle of the buoy	30	5	70	°

Table 6-1 Ranges of the size-related variables

The ranges of two variables generate in total 72 buoy designs with these combinations of size-related variables. To select the most optimized buoy, there will be several phases to test these combinations. In the following subsections, the optimization will be performed with the order of these phases.

6.2.1 Stationary Draft

The combinations of size parameters determine the stationary draft of the buoy. According to the limitation of the criterion (3), some of the combinations should be excluded. Table 6-2 shows the results of the stationary draft for each combination.

Stationary draft [m]		Maximum diameter [m]							
		7	7.5	8	8.5	9	9.5	10	10.5
Hull angle [°]	30	2.81	2.78	2.74	2.70	2.66	2.61	2.57	2.52
	35	2.73	2.68	2.63	2.57	2.52	2.46	2.41	2.36
	40	2.63	2.56	2.50	2.44	2.38	2.32	2.26	2.21
	45	2.51	2.44	2.37	2.30	2.24	2.18	2.13	2.07
	50	2.39	2.32	2.25	2.18	2.12	2.06	2.01	1.96
	55	2.28	2.20	2.13	2.06	2.00	1.95	1.90	1.85
	60	2.17	2.09	2.02	1.96	1.91	1.86	1.81	1.77
	65	2.07	2.00	1.93	1.87	1.82	1.77	1.73	1.69

	70	1.98	1.91	1.85	1.80	1.75	1.70	1.66	1.63

Table 6-2 Results of the stationary draft for each combination (Phase 1)

Results from Table 6-2 show that in total 51 combinations (shaded with green color, same as below) satisfy the limitation of the criterion (3). Therefore, from the remaining combinations, we can further search for the most optimized combination by performing the numerical simulation, where the related inputs are given in Table 6-3.

Time-step length	0.01	s
Simulation duration	100	s
Total length of the level ice	5050	m

Table 6-3 Related inputs of the simulation

The simulation duration is ensured to be sufficiently long for the level ice to fail at least two cycles due to bending, while the buoy can reach its maximum pitch angle and maximum horizontal displacement. The level ice is sufficiently long to ensure that the level ice has sufficient momentum to keep its velocity relatively constant after the bending failure.

6.2.2 Normal Ice Condition

To satisfy the criterion (4), critical pitch angles that the upward-sloping hull is not submerged into water for each combination are needed to be discovered. The corresponding results are shown in Table 6-4.

Critical submerging pitch angle [°]		Maximum diameter [m]							
		7	7.5	8	8.5	9	9.5	10	10.5
Hull angle [°]	30	-	-	-	-	-	-	-	-
	35	-	-	-	-	-	-	-	1.53
	40	-	-	-	-	1.57	2.18	2.71	3.16
	45	-	-	1.85	2.63	3.28	3.81	4.25	4.61
	50	1.74	2.78	3.62	4.30	4.84	5.27	5.62	5.89
	55	3.61	4.53	5.25	5.81	6.24	6.56	6.81	6.98
	60	5.36	6.14	6.72	7.15	7.47	7.68	7.83	7.92
	65	6.96	7.59	8.03	8.34	8.54	8.66	8.71	8.72
	70	8.38	8.86	9.16	9.35	9.45	9.47	9.45	9.39

Table 6-4 Critical submerging pitch angle (Phase 2)

The results of the maximum pitch angle under the normal ice condition (0.1 m/s) during the simulation are listed in Table 6-5.

Maximum pitch angle [°]		Maximum diameter [m]							
		7	7.5	8	8.5	9	9.5	10	10.5
Hull	30	-	-	-	-	-	-	-	-

angle [°]	35	-	-	-	-	-	-	-	5.38
	40	-	-	-	-	7.29	6.03	5.42	4.94
	45	-	-	8.69	7.49	6.79	5.90	4.71	3.92
	50	8.89	8.22	7.34	7.98	6.23	5.74	5.13	16.91
	55	8.58	7.62	6.32	6.63	5.24	4.98	8.38	5.30
	60	7.34	6.98	6.07	6.97	5.20	5.15	5.95	9.96
	65	6.82	6.02	7.45	5.57	4.68	7.21	*	*
	70	7.28	7.24	*	6.63	7.67	10.09	*	*

Table 6-5 Results of the maximum pitch angle (Phase 2)

The results from Table 6-5 can be compared with those in Table 6-4. According to the criteria (1) and (4), there are 20 combinations qualified in this test. ("*" indicates that the buoy overturned during the simulation, same as below.)

To check if the results satisfy the criterion (5), the maximum horizontal displacements from qualified combinations are recorded in Table 6-6.

Maximum horizontal displacement [m]		Maximum diameter [m]							
		7	7.5	8	8.5	9	9.5	10	10.5
Hull angle [°]	30	-	-	-	-	-	-	-	-
	35	-	-	-	-	-	-	-	-
	40	-	-	-	-	-	-	-	-
	45	-	-	-	-	-	-	-	4.53
	50	-	-	-	-	-	-	4.82	-
	55	-	-	-	-	4.70	4.83	-	4.29
	60	-	-	4.28	4.59	4.48	4.17	4.35	-
	65	4.20	3.85	4.58	4.62	4.00	3.42	-	-
	70	4.46	4.36	-	4.71	4.23	3.53	-	-

Table 6-6 Results of the maximum horizontal displacement (Phase 2)

From the results above, one can notice that the maximum horizontal displacements from only 13 combinations are lower than the limit that specified in the criterion (5), which is 4.5 m. Therefore, there are 13 qualified combinations in this phase.

6.2.3 Extreme Ice Condition

To further examine the performance of the buoys with qualified combinations, one of the solutions is to increase the ice velocity, for instance, 0.2 m/s, to simulate an extreme ice condition. To satisfy the criterion (6), a series of numerical simulation is performed. The results of the maximum pitch angle for each combination under the extreme ice condition (0.2 m/s) are listed in Table 6-7.

Maximum pitch angle [°]		Maximum diameter [m]							
		7	7.5	8	8.5	9	9.5	10	10.5
Hull angle [°]	30	-	-	-	-	-	-	-	-
	35	-	-	-	-	-	-	-	-
	40	-	-	-	-	-	-	-	-
	45	-	-	-	-	-	-	-	-
	50	-	-	-	-	-	-	-	-
	55	-	-	-	-	-	-	-	9.20
	60	-	-	11.77	-	11.04	7.97	11.66	-
	65	17.04	11.67	-	-	*	*	-	-
	70	18.16	20.67	-	-	20.17	*	-	-

Table 6-7 Results of the maximum pitch angle (Phase 3)

The results from Table 6-7 can be compared with those in Table 6-7. According to the criteria (1) and (6), there are 6 combinations qualified in this test.

To check if the results satisfy the criterion (7), the maximum horizontal displacements from qualified combinations are recorded in Table 6-8.

Maximum horizontal displacement [m]		Maximum diameter [m]							
		7	7.5	8	8.5	9	9.5	10	10.5
Hull angle [°]	30	-	-	-	-	-	-	-	-
	35	-	-	-	-	-	-	-	-
	40	-	-	-	-	-	-	-	-
	45	-	-	-	-	-	-	-	-
	50	-	-	-	-	-	-	-	-
	55	-	-	-	-	-	-	-	5.31
	60	-	-	6.59	-	6.59	9.74	6.01	-
	65	-	6.42	-	-	-	-	-	-
	70	-	-	-	-	-	-	-	-

Table 6-8 Results of the maximum horizontal displacement (Phase 3)

From the results above, one can notice that the maximum horizontal displacements from only 5 combinations are lower than the limit that specified in the criterion (7), which is 7.5 m. Therefore, there are only 5 buoy designs satisfy the design criteria listed in Section 6.1. The result so far indicates that the 5 qualified buoy designs can perform well both under the normal and extreme ice conditions.

6.2.4 Buoy Weight

Since the aim of the optimization is to find the moored buoy with minimized dimensions, with all the design criteria satisfied, one can check the weights of qualified buoy designs. The buoy design with the lowest weight will be the most optimized design. The buoy weights of all the qualified designs are listed in Table 6-9.

Buoy weight [t]		Maximum diameter [m]							
		7	7.5	8	8.5	9	9.5	10	10.5
Hull angle [°]	30	-	-	-	-	-	-	-	-
	35	-	-	-	-	-	-	-	-
	40	-	-	-	-	-	-	-	-
	45	-	-	-	-	-	-	-	-
	50	-	-	-	-	-	-	-	-
	55	-	-	-	-	-	-	-	105.69
	60	-	-	66.34	-	82.00	-	99.19	-
	65	-	61.27	-	-	-	-	-	-
	70	-	-	-	-	-	-	-	-

Table 6-9 Buoy weights of qualified designs (Phase 4)

From Table 6-9, one can discover that the buoy design with the hull angle of 65°, and the maximum diameter of 7.5 m has the lowest weight among 5 qualified buoy designs, and thus, we can conclude that this design is the most optimized buoy design based on the design criteria and the size ranges of our research.

6.3 Conclusion

Based on the current criteria, the most optimized buoy design has been chosen, and its parameters are summarized in Table 6-10.

Maximum diameter	$D_{s,max}$	7.5	m
Minimum diameter	$D_{s,min}$	5.63	m
Waterline diameter	$D_{s,wli}$	7.03	m
Height	H_s	3	m
Draft	d_s	2.00	m
Displaced water volume	$V_{d,s}$	59.77	m^3
Weight	m_s	6.13×10^4	kg
Downward-sloping hull angle	α	65	°
Upward-sloping hull angle	θ	28.20	°
Moment of inertia	$I_{n,s}$	4.30×10^5	$kg\cdot m^2$
Material density	ρ_s	7850	kg/m^3
Surface area	S_s	126.09	m^2
Equivalent hull thickness	t_s	0.0619	m
Second moment of area	$I_{t,s}$	2.06	m^4
Radius of gyration	$R_{g,s}$	2.65	m

Table 6-10 Parameters summary of the optimized buoy design

This thesis only provides one of the examples of the method of optimizing a moored buoy. However, the optimization process and results can be different based on different practical situations and requirements.

7

CONCLUSIONS AND RECOMMENDATIONS

7.1 Conclusions

The current study focuses on the investigation of the interaction between the level ice and the moored buoy, which is a conventional research area involving the Arctic environment. The interaction between the level ice and the moored buoy is investigated based on two-dimensional numerical modeling and simulation. In fact, the modeling and simulating methods employed in this thesis can be generalized to any other types of floating structures. This thesis, in particular, chose the moored buoy as the research object.

During the study, several research methods and concepts are introduced, which includes:

- Compliant contact algorithm
- Lagrange multiplier formulation
- Catenary mooring system

The compliant contact algorithm, as a variant of the non-smooth discrete element method (NDEM), is capable of describing any compliant contacts in the system, including ice-ice contact and ice-structure contact.

The Lagrange multiplier formulation is applied in order to solve the model, during the simulation, the formulation is solved by Gauss-Seidel method for each time-step. The formulation has the advantage to be able to solve the implicit forces of the system.

The catenary mooring system is the most common type of mooring system employed to the buoy in shallow water, which provides the buoy with significant stationary stability.

Based on the above methods, the numerical model is constructed, which consists of the level ice model, and the moored buoy model. The level ice model is built as a beam with multiple elements, while the moored buoy model is constructed as a rigid body. Besides, several mechanisms are employed to handle the interaction between the level ice and buoy, which includes:

- Ice compressive failure
- Ice bending failure
- Friction

The ice compressive failure happens directly due to the ice-structure contact, which is the essential failure type during the ice-structure interaction. However, since the buoy itself moves significantly after the contact, the extent of the ice compressive failure (penetration) is usually small in the current research.

The ice bending failure happens for the reason that the ice contacts with the downward-sloping hull of the buoy. Since that the buoy is a small-scale structure in terms of dimension, for low ice velocity, the ice does not usually break due to bending during the first ice-structure contact phase. Instead, the level ice pushes the buoy horizontally, which changes the tensions in mooring lines. When the opposite two mooring lines have sufficiently large tension difference, the restoring force will be large enough to make the ice bending stress exceed its failure limit, and thus the bending failure occurs.

The friction generally exists during the ice-structure contact, which affects both the level ice and the buoy. The friction is the result of relative motions at the contact surface, which based on the current research, is modeled as the continuous variation of contact points during the contact phase.

Following that, the thesis carries out a series of determinations of model parameters regarding the numerical model, which includes:

- The level ice
- The (pre-designed) buoy
- The mooring system

The above parametric studies are all based on the Arctic environmental situation of the Svalbard archipelago. After the parametric studies accomplished, the model has a certain degree of capability to simulate the practical situation.

To ensure the correctness and accuracy of the numerical model, for each mechanism that relies on the Lagrange multiplier formulation, a corresponding verification is carried out. The referring objects of verification generally include:

- Analytical solutions
- Solutions obtained by the ode45 solver
- Previous results of numerical simulations

With the verification process correctly accomplished, the numerical model is proved sufficiently effective and accurate, and can be used to perform further optimization for the buoy design.

The thesis provides one of the examples of the process of optimization, in order to design a buoy with smaller weight but with sufficient stability under certain ice conditions. Furthermore, with similar design criteria and optimization process, one can design and optimize a different type of offshore structure in the Arctic environment based on the provided numerical model.

7.2 Recommendations

The following aspects are recommended to improve or complement the current numerical model:

Modeling of broken ice:
The current numerical model does not present the broken ice and its influence due to the time limit. Generally, the broken ice continuously contacts with the buoy after the level ice fails either due to compression or bending. Besides, the current modeling method allows the straightforward implementation of broken ice. Although the influence of the broken ice is relatively smaller considering that the ice-buoy interaction produces a relatively small amount of broken ice, it is recommended to be taken into account and added to the model, in order to further improve the capability to simulate the practical situation in the Arctic environment.

Wind and current loads:
The current research only considers the ice load as the only load type subject on the buoy. However, in the Arctic environment, the wind load influences the buoy especially on the superstructure of the buoy; the current load influences the underwater part of the buoy and the mooring chains. Therefore, it is recommended to further research the influences of the Arctic wind and current loads.

Different types of structure:
The current study chose the buoy as the object of research. The buoy is generally considered as a small-scale or medium-scale floating structure, which usually has significant motions under environmental loads. It has certain advantages in terms of design optimization, which, however, weakens the extent of failures of the level ice. Therefore, if the further research intends to focus more on ice failures, it is recommended to employ a larger-scale of floating structure.

Interaction between the buoy and its anchoring floating structure:
Since the buoy is one component of the single point mooring (SPM) system, it is in fact connected to its anchoring floating structure, such as an FPSO unit. The current research does not focus on the interaction between the buoy and its anchoring structure. Therefore, it would be interesting to consider this interaction into the numerical model, to further research the feasibility and advantages in terms of the SPM solution.

Three-dimensional expansion:
The current numerical model is constructed mainly based on a two-dimensional plane, which limits the simulation in terms of degrees of freedom. To further improve the model and yield results with better accuracy, it is recommended to expand the model to the three-dimensional space.

REFERENCES

[1] SOFEC. (2009). Retrieved from https://www.oilandgasmiddleeast.com/

[2] Wikipedia. (2018). Retrieved from https://en.wikipedia.org/wiki/Svalbard

[3] M. Servin, D. Wang, C. Lacoursière and K. Bodin. (2014). *Examining the smooth and nonsmooth discrete element approaches to granular matter*. UMIT Research Lab, Umeå University, Umeå, SE-90187, Sweden.

[4] Vincent Duindam, Stefano Stramigioli. (2013). *Modeling the Kinematics and Dynamics of Compliant Contact*. Drebbel Institute for Mechatronics, University of Twente, The Netherlands.

[5] Newmark, Nathan M. (1959). *A method of computation for structural dynamics*. Journal of Engineering Mechanics, ASCE, 85 (EM3): 67–94.

[6] David Baraff. (1996). *Linear-Time Dynamics using Lagrange Multipliers*. Carnegie Mellon University, USA.

[7] Horn, Roger A.; Johnson, Charles R. (2012). *Matrix analysis*. Cambridge University Press.

[8] C. Siow, J. Koto, H. Yasukawa, A. Matsuda, D. Terada, C. Soares, and Muhamad Zameri bin Mat Samad. (2014). *Strength Analysis of FPSO's Mooring Lines*. The 1st Conference on Ocean, Mechanical and Aerospace, Pekambaru, Indonesia.

[9] "Catenary". (2003). Retrieved from Xahlee.org

[10] Marnix van den Berg. (2016). *A 3-D Random Lattice Model of Sea Ice*. SAMCoT, Norwegian University of Science and Technology, Norway.

[11] Renate van Vliet, Andrei V. Metrikine. (2017). *Derivation and verification of a lattice model for bending vibration of a plate*. Delft University of Technology, The Netherlands.

[12] J.M.J. Journée and W.W. Massie. (2011). *Offshore Hydromechanics, First Edition*, pp. 2-12. Delft University of Technology, The Netherlands.

[13] J.M.J. Journée and W.W. Massie. (2011). *Offshore Hydromechanics, First Edition*, pp. 10-8. Delft University of Technology, The Netherlands.

[14] *Ice Characteristics and Ice/Structure Interactions*. (2010). Bureau Veritas, Marine Division, France.

[15] *Ice Engineering*. (2006). Department of the Army, US Army Corps of engineers, USA.

[16] D. Blanchet, W. Spring, R.F. McKenna, G.A.N. Thomas. (2011). *ISO 19906: An International Standard for Arctic Offshore Structures*. OTC Arctic Technology Conference, Houston, Texas, USA.

[17] Horner, S. (1965). *Fluid Dynamic Drag, Practical Information on Aerodynamic Drag and Hydrodynamic Resistance*, pp. 440, Hoerner Fluid Dyn., Midland Park, N. J, USA.

[18] White, Frank. (2011). *Fluid Mechanics*, pp. 477-478. New York City, USA.

[19] Marnix van den Berg, Sveinung Løset. (2015). *A Concept Design For A Meso-Scale Floater To Measure Downward Bending Failure Ice Loads*. Sustainable Arctic Marine and Coastal Technology, Centre for Research-based Innovation, Norwegian University of Science and Technology, Trondheim, Norway.

[20] D.J. Auld, K. Srinivas. (2006). *Aerodynamics for students*. Aerospace, Mechanical & Mechatronic Engineering, University of Sydney, Australia.

[21] John J. Myers, Carl H. (1969). Holm, Raymond F. McAllister. *Handbook of Ocean and Underwater Engineering*. North American Rockwell Corporation, USA.

[22] *Boating Safety Study Guide*. (2018). Boat U.S. Foundation, Annapolis, Maryland, USA. Retrieved from https://www.boatus.org/study-guide/navigation/anchoring/

[23] C. Keijdener, H. Hendrikse, A. Metrikine. (2018). *The effect of hydrodynamics on the bending failure of level ice*. Delft University of Technology, The Netherlands.